

Serial ruptures of the San Andreas fault, Carrizo Plain, California, revealed by three-dimensional excavations

Jing Liu-Zeng, Yann Klinger, Kerry Sieh, Charles Rubin, Gordon Seitz

▶ **To cite this version:**

Jing Liu-Zeng, Yann Klinger, Kerry Sieh, Charles Rubin, Gordon Seitz. Serial ruptures of the San Andreas fault, Carrizo Plain, California, revealed by three-dimensional excavations. Journal of Geophysical Research : Solid Earth, 2006, 10.1029/2004JB003601 . insu-01302170

HAL Id: insu-01302170

https://insu.hal.science/insu-01302170

Submitted on 13 Apr 2016

HAL is a multi-disciplinary open access archive for the deposit and dissemination of scientific research documents, whether they are published or not. The documents may come from teaching and research institutions in France or abroad, or from public or private research centers.

L'archive ouverte pluridisciplinaire **HAL**, est destinée au dépôt et à la diffusion de documents scientifiques de niveau recherche, publiés ou non, émanant des établissements d'enseignement et de recherche français ou étrangers, des laboratoires publics ou privés.

Serial ruptures of the San Andreas fault, Carrizo Plain, California, revealed by three-dimensional excavations

Jing Liu-Zeng,[1,2,3] Yann Klinger,[1,2] Kerry Sieh,[1] Charles Rubin,[4] and Gordon Seitz,[5]

Received 27 December 2004; revised 15 August 2005; accepted 21 September 2005; published 28 February 2006.

[1] It is poorly known if fault slip repeats regularly through many earthquake cycles. Well-documented measurements of successive slips rarely span more than three earthquake cycles. In this paper, we present evidence of six sequential offsets across the San Andreas fault at a site in the Carrizo Plain, using stream channels as piercing lines. We opened a latticework of trenches across the offset channels on both sides of the fault to expose their subsurface stratigraphy. We can correlate the channels across the fault on the basis of their elevations, shapes, stratigraphy, and ages. The three-dimensional excavations allow us to locate accurately the offset channel pairs and to determine the amounts of motion for each pair. We find that the dextral slips associated with the six events in the last millennium are, from oldest to youngest, $\geq 5.4 \pm 0.6$, 8.0 ± 0.5, 1.4 ± 0.5, 5.2 ± 0.6, 7.6 ± 0.4 and 7.9 ± 0.1 m. In this series, three and possibly four of the six offset values are between 7 and 8 m. The common occurrence of 7–8 m offsets suggests remarkably regular, but not strictly uniform, slip behavior. Age constraints for these events at our site, combined with previous paleoseismic investigations within a few kilometers, allow a construction of offset history and a preliminary evaluation of slip- and time-predictable models. The average slip rate over the span of the past five events (between A.D. 1210 and A.D. 1857.) has been 34 mm/yr, not resolvably different from the previously determined late Holocene slip rate and the modern geodetic strain accumulation rate. We find that the slip-predictable model is a better fit than the time-predictable model. In general, earthquake slip is positively correlated with the time interval preceding the event. Smaller offsets coincide with shorter prior intervals and larger offset with longer prior intervals.

Citation: Liu-Zeng, J., Y. Klinger, K. Sieh, C. Rubin, and G. Seitz (2006), Serial ruptures of the San Andreas fault, Carrizo Plain, California, revealed by three-dimensional excavations, *J. Geophys. Res.*, *111*, B02306, doi:10.1029/2004JB003601.

1. Introduction

[2] Forecast of large earthquakes might be possible if theorists could constrain the range of plausible physical models with precise reconstructions of prior rupture histories, that is, the variations in timing and rupture magnitude of past events. Our understanding of the nature of earthquake repetition is hampered by a lack of long records of relevant high-quality data bearing on the behavior of past large ruptures. A myriad of models have been proposed to describe earthquake recurrence. Some models predict highly regular sequences [e.g., *Reid*, 1910; *Schwartz and Coppersmith*, 1984; *Sieh*, 1981, 1996; *Stuart*, 1986; *Tse and Rice*, 1986; *Ward and Goes*, 1993; *Rice*, 1993; *Rice and Ben-Zion*, 1996; *Lapusta et al.*, 2000], whereas others predict highly irregular behavior [e.g., *Bak and Tang*, 1989; *Carlson and Langer*, 1989; *Ito and Matsuzaki*, 1990; *Huang et al.*, 1992; *Shaw*, 1995; *Ben-Zion*, 1996; *Cochard and Madariaga*, 1996; *Ward*, 1997; *Lyakhovsky et al.*, 2001; *Shaw and Rice*, 2000]. The lack of determinative data makes it difficult to narrow down the list of feasible models.

[3] Our limited understanding of earthquake recurrence also influences the practice of seismic hazard analysis. The characteristic earthquake model was considered such a simple yet reasonable idealization that it was extensively applied in seismic hazard assessment [e.g., *Working Group of California Earthquake Probabilities*, 1988, 1995]. However, one should be aware of our reliance on tenuous assumptions of source recurrence in these approaches. For example, it was believed that seismicity on a fault could be represented realistically by a repeating characteristic rupture and that slip patterns along large historical ruptures reflect along-strike differences in fault friction [e.g., *Stuart*, 1986; *Rundle*, 1988; *Ward and Goes*, 1993]. In reality, we have only very sparse data to

[1]Division of Geological and Planetary Sciences, California Institute of Technology, Pasadena, California, USA.
[2]Laboratoire de Tectonique, Institut de Physique du Globe Paris, Paris, France.
[3]Now at the Institute of Tibetan Plateau Research, Chinese Academy of Sciences, Beijing, China.
[4]Department of Geological Sciences, Central Washington University, Ellensburg, Washington, USA.
[5]Department of Geological Sciences, San Diego State University, San Diego, California, USA.

Copyright 2006 by the American Geophysical Union.
0148-0227/06/2004JB003601$09.00

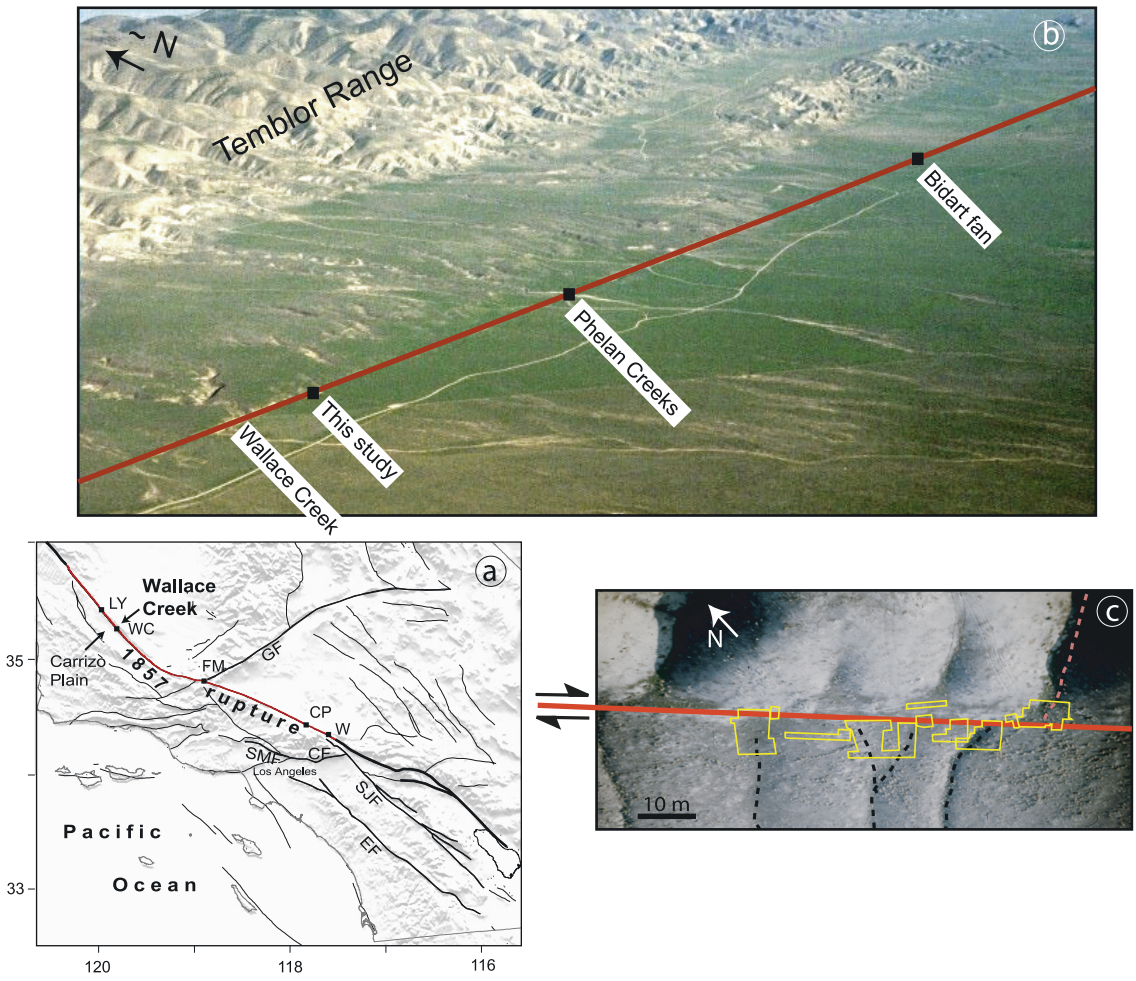


Figure 1. Location of the Wallace Creek trench site. (a) Active faults in California, with 1857 earthquake rupture on the San Andreas fault highlighted in red. Abbreviations of some paleoseismic investigation sites along the San Andreas fault: LY, Las Yeguas; WC, Wallace Creek; FM, Frasier Mountain; CP, Pallett Creek; W, Wrightwood. Abbreviations of faults: GF, Garlock fault; SMF, Sierra Madre fault; CF, Sierra Madre-Cucamonga fault; SJF, San Jacinto fault and EF, Elsinore fault. (b) Oblique aerial photo of the San Andreas fault near the Wallace Creek site showing locations of two previous investigations. Photo by T. Rockwell. (c) Close-up aerial oblique photo of the trench site. Thin dashed lines indicate geomorphic stream channels. Polygons in yellow denote locations of excavation volumes. A narrow excavation on the upstream side is placed in front of a secondary channel. The exposures in this trench show that the incision is minor and not enough to be a source channel.

support this idea [*Lindvall et al.*, 1989; *Sharp et al.*, 1982].

[4] Paleoseismology has contributed to understanding serial fault ruptures by documenting the history of earthquakes at specific locations along faults worldwide [e.g., *McCalpin*, 1996; *Yeats et al.*, 1997]. However, most paleoseismic investigations uncovered only the times of paleoearthquakes. Well-documented examples of slip measurements for these earthquakes are still rare. High-quality data rarely span more than two earthquake cycles [*Sieh*, 1996, and references therein]. Longer records of paleoearthquake slips [e.g., *Schwartz and Coppersmith*, 1984; *Sieh*, 1984; *Pantosti et al.*, 1996; *Ran et al.*, 1997; *Weldon et al.*, 2002] are, however, inaccurate or mostly based on indirect evidence; for example, the similar displacement of paleoseismic events on the Wasatch fault was inferred from the heights of colluvial wedges caused by these events.

[5] Thus our goal in this study is to document details of several sequential offsets from a single site on the Carrizo section of the San Andreas fault (Figure 1). We have recently summarized this work [*Liu et al.*, 2004]. Here we present a more complete documentation of our results, including efforts to date the offsets and speculate about the slip history. At the site, a feeder channel cuts a late Pleistocene alluvial fan on the upstream side of the fault. On the downstream side, several small channels have been offset dextrally from the feeder channel and sequentially abandoned. We have conducted three-dimensional excavations across these channels. Using offset channels as piercing lines, we have recovered an accurate record of offsets for six sequential ruptures. Sparse reliable radiometric dates

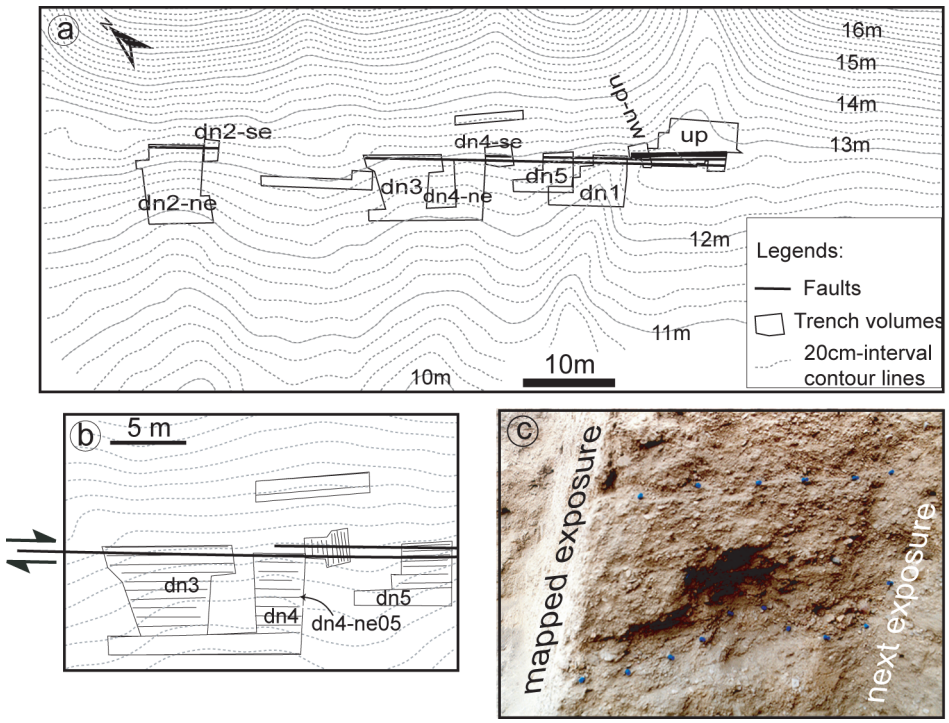


Figure 2. Map of excavations at the site. (a) Map of the 11 separate volumes that were excavated. The seven that exposed channels are labeled "up" or "dn," depending on their location upstream or downstream from the fault. The suffixes "ne" and "se" indicate the direction of serial cuts within the excavation. (b) An example of the arrangement of mapped exposures within the excavated volumes. (c) Photo showing the procedure that we use channel stratigraphy to check for evidence of a fault between two consecutive cuts.

do not allow us to determine accurately their dates from this site alone. However, previous paleoseismic studies at sites within several kilometers, the Phelan Creeks and the Bidart fan sites, have yielded tighter constraints on the occurrence times, but not the offsets of paleoruptures (Figure 1b) [*Prentice and Sieh*, 1989; *Grant and Sieh*, 1994; *Sims*, 1994; J. D. Sims et al., unpublished manuscript, 1994]. A combination of these studies improves the slip time sequence.

[6] We organize the paper into 10 sections: Sections 1, 2, and 3 set forth the nature of the study, the background, previous work and methodology. Section 4 is a lengthy detailed description of the stratigraphy and morphology of channels exposed in the excavations. Section 5 gives the evidence for correlation of 6 upstream and downstream pairs of offset channels. In section 6 we calculate the offset values. In section 7 we derive the rupture sequence and address the question of whether each offset is a single rupture event. Section 8 provides radiocarbon constraints on the offset events. Then, in section 9 we proceed to create an offset history on the basis of the sequence of offsets and our best estimates of the dates of events. Finally, in section 10 we discuss the implications of the sequence of offsets at the site. We suggest that the casual readers of this paper focus their attention on the figures in the sections 2, 3, 4, 7, and 8, and focus on sections 5, 6, 9, and 10.

2. Site Description

[7] The Carrizo Plain is an arid to semiarid intermontane closed basin about 80 km northeast of the California coastline. Ephemeral streams, dry except during local cloudbursts in the dry season or during large Pacific storms in the wetter winter months, incise the flanks the Temblor Range on the northeast. In the vicinity of Wallace Creek (Figure 1b), the main surface is an apron of late Pleistocene alluvial fans derived principally from Miocene marine deposits of the Temblor Range [*Dibblee*, 1973]. The fans were aggrading through the period from 33 ka to at least 19 ka [*Sieh and Jahns*, 1984]. This surface became inactive about 13,250 years B.P. Entrenchment of the late Pleistocene surface by active streams has continued throughout the Holocene epoch. At Wallace Creek the vertical component of motion on the San Andreas fault has been northeast side up, resulting in the present south facing 8- to 9-m-high scarp. This section of the San Andreas fault ruptured during the latest large earthquake in 1857 with several meters of right-lateral offset [*Agnew and Sieh*, 1978; *Sieh*, 1978].

[8] The Carrizo section of the San Andreas fault is an ideal place to determine whether or not a fault segment can experience similar amounts of slip through many earthquake cycles. First of all, along much of this segment the fault trace is geometrically simple and well expressed. Secondly, beheaded channels indicating various amounts of offset are common. Thirdly, the potential to discriminate individual offsets has been known [*Wallace*, 1968; *Sieh*, 1978; *Sieh and Jahns*, 1984].

[9] We refer to our excavation site as the "Wallace Creek paleoseismic site," because it is just a few hundred meters southeast of Wallace Creek (Figure 1b), where *Sieh and Jahns* [1984] made the first determination of a slip rate

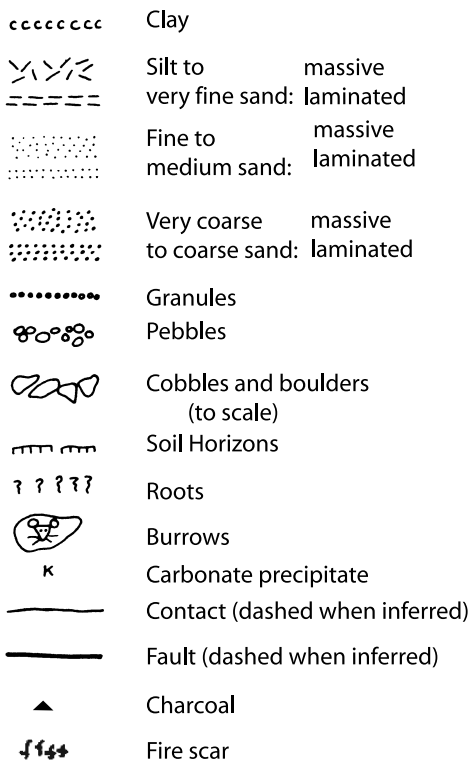


Figure 3. Lithologic and other symbols used in documenting the exposures. Modified from *Grant and Sieh* [1994].

along the San Andreas fault, ~34 mm/yr. The site is at the outlet of one of several small gullies that cut the late Pleistocene alluvial fan but extend only a hundred meters or so upstream. The particular small drainage that we chose was first studied by *Wallace* [1968] and then by *Sieh* [1978] (site 25, 35°16′10″ 119°49′05″). *Sieh* [1978] measured the offsets of the beheaded channels to be 8.7 ± 1.4 m, 24.1 ± 1.4 m, 32.0 ± 2.0 m and 56.4 ± 2.9 m, from the youngest to the oldest.

[10] However, these purely geomorphic estimations of channel offsets are plagued with ambiguities. First, colluviation at the base of the scarp has buried these small downstream gullies partially, so their precise geometry near the fault is obscure. Thus geomorphic measurements of offsets are imprecise. Another source of uncertainty in the interpretation of geomorphic measurements is the possibility of channel piracy. Strike-slip motion along a fault can bring a downstream channel, whose source is far away, into alignment with a different upstream channel [*Wallace*, 1968; *Gaudemer et al.*, 1989; *Huang*, 1993; *Schumm et al.*, 2000]. If unrecognized, such piracy can lead to mismatching of offset channels and incorrect measurements of offset.

3. Methods

[11] Guided by the geomorphic observations, we conducted three-dimensional excavations on either side of the San Andreas fault and matched channels based on the similarity in subsurface channel morphology and stratigraphy. Basically, we have explored 11 volumes: three on the upstream side of the fault, and eight on the downstream side (Figure 2a). The excavated volumes downstream from the fault exposed relationships along a 50-m length parallel to the fault and northwest of the source channel. They were placed to reveal all downstream channel segments within the 50-m fault-parallel length of the channel outlet.

[12] Most of the volumes were excavated progressively. That is, we began by excavating a narrow trench by hand, 4–5 m from and parallel to the fault, astride a gully. After mapping both walls of these initial trenches, we cut into the wall closest to the fault, creating another exposure closer to the fault. After mapping this new face, we once again cut a new exposure, still closer to the fault. Subsequent faces were cut closer and closer to the fault by increments of 50 to 60 cm. Near the fault, the increments were commonly only about 20 cm (Figure 2b). In places where channels flowed nearly parallel to the fault zone, trench cuts would be oriented fault-normal. Between parallel cuts near the fault zone, we would cut a ~50-cm-wide notch and use channel stratigraphy to check for faults between the faces (Figure 2c). In this manner, we carefully followed each potential piercing line into the fault zone. Although making series of successive cuts was time consuming, it greatly reduced the uncertainty in interpreting channel stratigraphy. Contacts that were ambiguous in one wall would often be clear in the next.

[13] Our choice of 60- to 20-cm increments represented a compromise between the demands of rigor and logistics. These increments were small enough to reveal the continuation of channel stratigraphy between cuts. Using smaller increment would undoubtedly have revealed more detail in channel variation, but would also have increased the time and effort required. Instead of mapping cuts at smaller increments, we chose to inspect important channel contacts (e.g., channel thalwegs and sharp edges) as we dug from one cut to the next.

[14] The fault-parallel orientation of progressive cuts is optimal for reconstruction of channel stratigraphy and offset markers. Yet, fault-perpendicular cuts are optimal for mapping the geometry of the fault zone. Although most of our excavations were fault-parallel, auxiliary fault-perpendicular trenches in areas away from the channels revealed the location of important faults.

[15] The name of each exposure reflects the name of the volume it belonged to, when in the sequence it was cut, and the direction of cutting. For example, exposure dn4-ne05 was the fifth cut within downstream volume 4, and it was on the northeastern wall of the volume. Exposures were cleaned, surveyed with a Total Station, using the same reference frame, and mapped at 1:15 scale (except 1:20 scale for trench dn1). Symbols used in mapping appear in Figure 3. Strata within the channels were correlated from one exposure to the next based on lithologic similarity, stratigraphic position and elevation of the upper and lower contacts. We later reconstructed the three-dimensional geometry of channels and faults from dense survey data. High-precision channel geometry and location thus gave greatly refined slip measurements.

4. Channel Stratigraphy and Morphology

[16] We assign the downstream channels letter names (from a to l, Figure 4), where a is closest to the mouth of source channel and l is farthest. Upstream channels are named numerically from 1 to 9, from youngest to oldest.

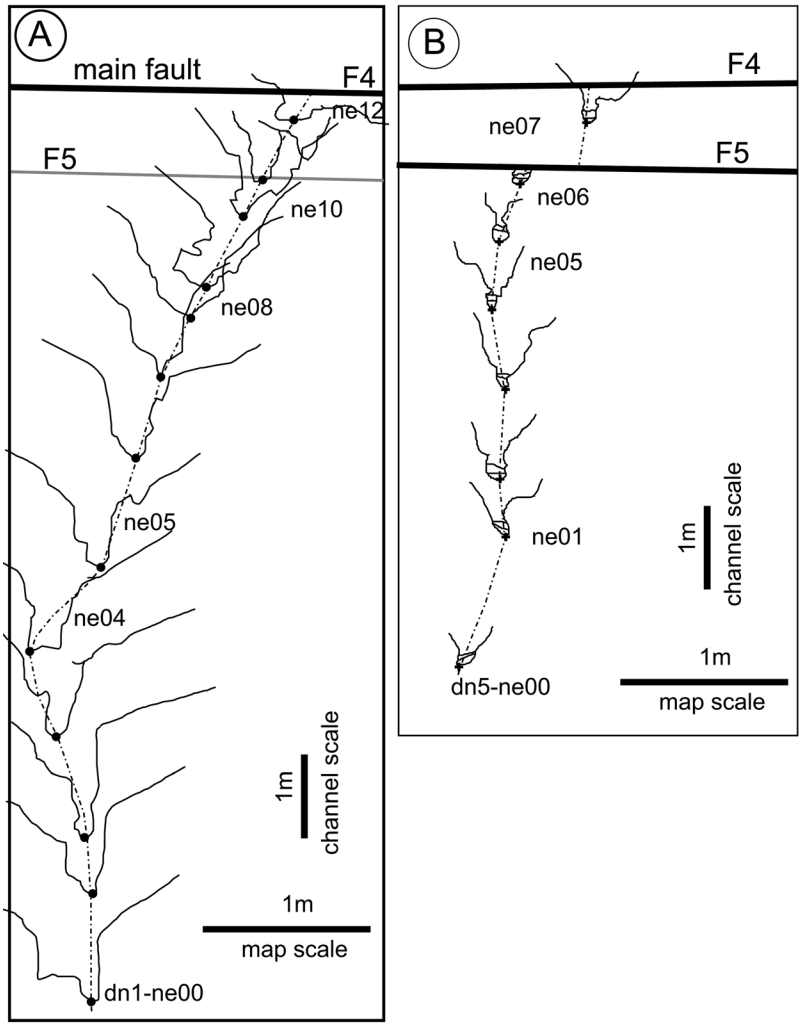


Figure 4. Summary of the results of excavations of all channels. (f) Locations of the channels and excavated volumes in map view. Downstream channels are assigned letters, from a to l, southeast to northwest. Upstream channels are numbered from 1 to 9, from youngest to oldest. Major fault strands F1 through F6 are correlated from exposure to exposure on the basis of the projection of strikes, relative position, and the spacing between them. Gray polygons indicate the perimeters of excavated volumes. (a)–(e) Detailed maps of the deepest thalwegs of downstream channels and their meanders. The cross sections appear on the plan view map to illustrate the change in channel shape that occurs along the stream profile. The viewing direction in each cross section is toward upstream, and the deepest thalweg of the channel in each exposure appears as a dot in its correct geographic location. (g) Thalwegs of upstream channels in map view. Symbols connected with dashed lines indicate the position of the thalwegs in each mapped exposure. Simplified cross sections of downstream channels from each mapped exposure show the variability in channel shape and stratigraphy. Numbers at the base of Figure 4g indicate the horizontal offsets of channels 1 through 6 across fault F1 and F2. The shading between F1 and F2 indicates that F2 is a shallow branch of F1.

The stratigraphic sequence of the channels generally revealed a complex history of cuts and fills. Major units were defined by their textures and the prominence of their lower contacts, which were generally major erosional surfaces. Each major unit contained multiple subunits. Because of limited space, we have put the maps and descriptions of channel stratigraphy of most channels as in the auxiliary material[1] (Figures S1–S15).

[1]Auxiliary material is available at ftp://ftp.agu.org/apend/jb/2004JB003601.

4.1. Downstream Channels

[17] The substrate underlying all the downstream channels was a massive indurated and matrix-supported pebbly sand and silt, interbedded with sorted gravelly and sandy lenses. A more than 1-m-thick pedogenic carbonate horizon (B_k) developed within this unit and had penetrated into the matrix, consistent with its late Pleistocene age [*Sieh and Jahns*, 1984].

[18] The distinction between the late Pleistocene fan and recent channel deposits manifests itself in three ways:

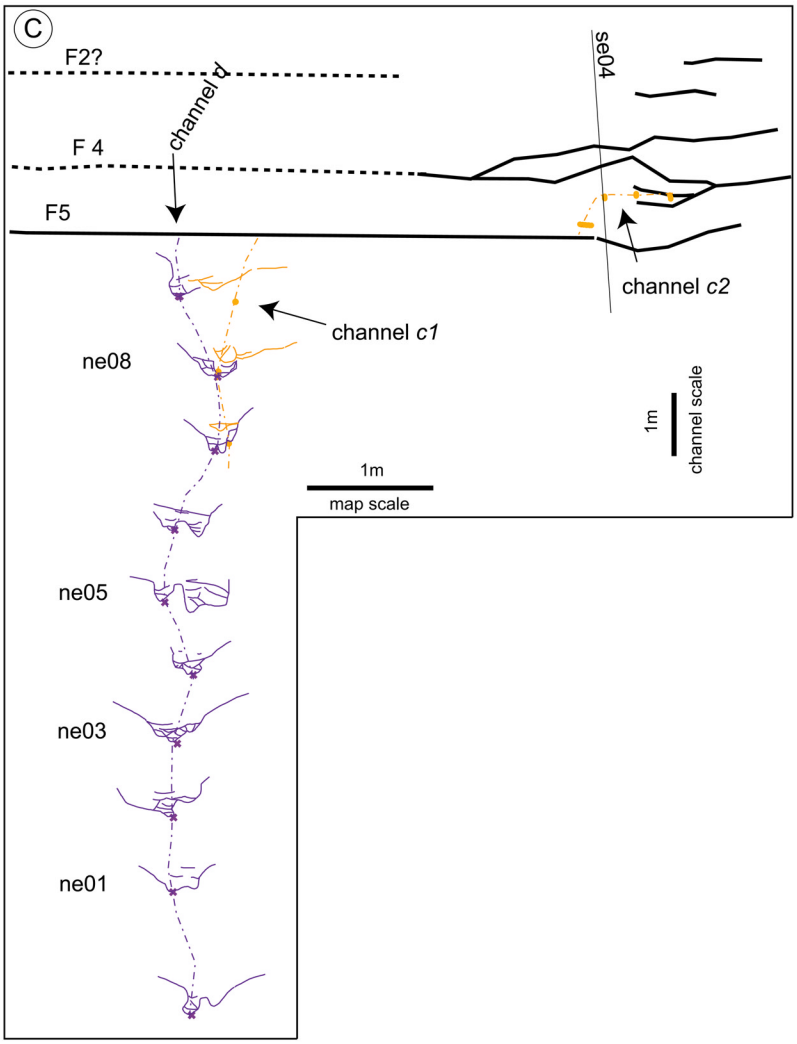


Figure 4. (continued)

[19] 1. The colors of the two units differ. The channel deposits are usually darker than the older underlying unit.

[20] 2. The edges of the channels, especially in the lower part, are generally clear. However, finding the channel walls was sometimes tricky, especially in the upper part of the channel, where deposits filling the channel were commonly colluvium, derived from collapse of the upper channel wall and thus compositionally similar to the substrate material.

[21] 3. Lenses of well-sorted sand and gravel within the younger channels are traceable from cut to cut. These well-sorted sand and gravel layers within the channels, when they can be traced over several meters in the channels, provided good markers for stratigraphic correlation from cut to cut in each trench.

4.1.1. Channel a

[22] Channel a was the southernmost channel on the downstream side of the fault (Figure 4f). In map view (Figure 4a), the deepest thalweg of channel a curved right as one views it looking toward the fault. It had a prominent right step in the middle of its course, between exposure ne04 and ne05. This step was demonstrably not an offset across a minor fault. A large cobble, 25 cm long and 3–10 cm thick, blocked the channel in exposure ne04 (Figure S2). The thalweg skirted the blockage on the left. Figure 4a also shows the simplified cross-sectional outlines of channel a derived from our mapping of sequential channel walls. Although channel a cut into the landscape only about 0.5 m, its deepest thalweg (the deepest part of the channel) was 1.5 m or so deeper.

4.1.2. Channel b

[23] Channel b appeared in the excavation volume 5–6 m northwest of channel a (Figure 4f). Any geomorphic evidence for this channel was lost following the incision of channel a. Its presence was only hinted at by the asymmetry of the banks of channel a near the fault, and the slight bending of a couple of topographic contour lines near the fault.

[24] Channel b was distinctly different than channel a. In all exposures, it was narrow, with a bottleneck in the channel walls some centimeters up from the thalweg (Figure 4b). The thalweg of channel b ran straight into the fault. Its lack of curvature is additional evidence that the bend in younger channel a was not tectonic in origin. Secondary fault F5 cut through exposure ne06 (Figure 4b). In this exposure, the fault dipped into the exposure such that the channel was missing above the fault. This secondary

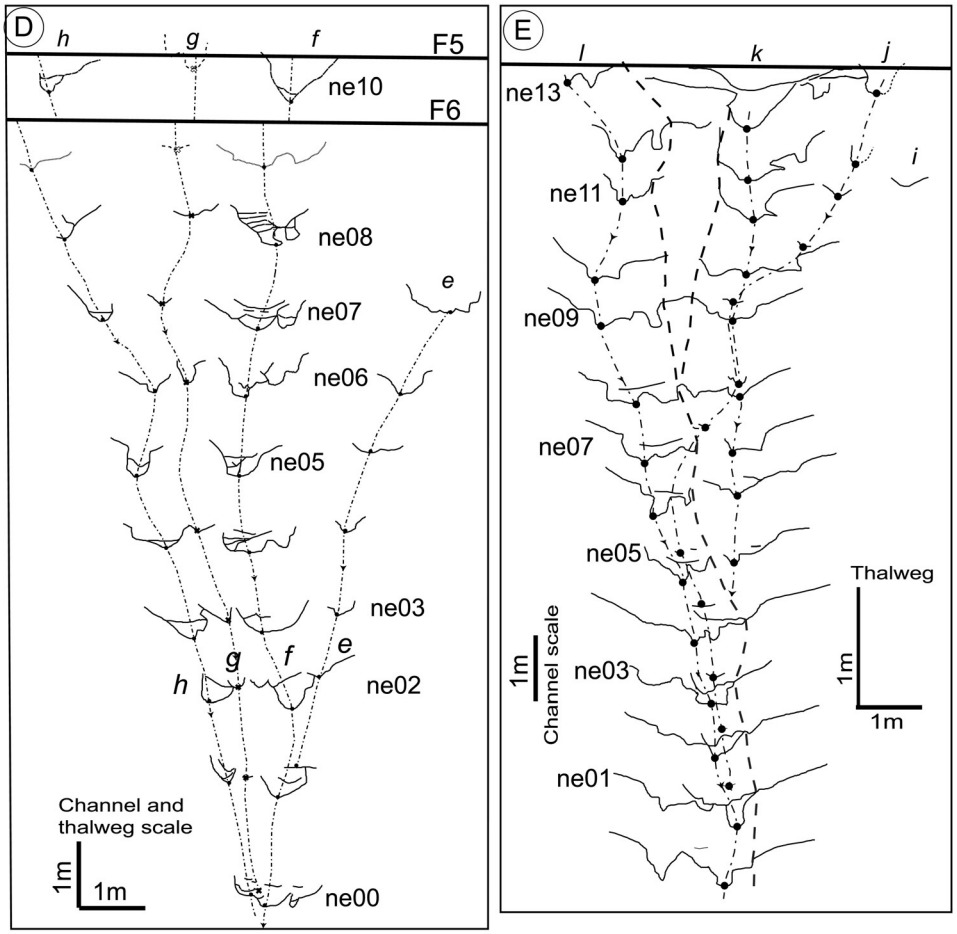


Figure 4. (continued)

fault did not disrupt younger channel a and thus was active only between filling of channel b and cutting of channel a.

4.1.3. Channels c and d

[25] We found a set of two channels, c and d, 5 to 11 m northwest of channel b (Figures 4c and 4f). In plan view, channel d was nearly perpendicular to and ran straight into fault F5. Channel d was 1 to 1.2 m deep and generally W-shaped, which was the result of two major phases of scour and fill (Figure 5). The second major down-cutting event widened channel d, mostly by scouring the southern bank. This cutting extended as deep as the first incision, thus forming a second thalweg less than a meter southeast of the first.

[26] Channel c was more complicated. It consisted of two segments, c1 and c2, on either side of fault F5. In plan view, channel c1 diverged from the path of channel d in a right-lateral sense within a meter of the fault (Figure 4c). In cross sections, channel c1 cut the channel d in the upper right corner. Best exposed in ne08, channel c1 consisted of a semicircular erosion surface filled with gravel and sand (labeled ''c-10'' in Figure 5). The deposits within the channel were thickest near the fault and diminished quickly to zero farther downstream (Figure 4c). Channel c2, was a 1.5-m-long channel segment within in the fault zone and to the southeast of c1. It had a cylindrical shape and was about 40–50 cm wide in cross sections perpendicular to the fault zone (e.g., dn4-se04; Figure 6). The bottom 30 cm of the channel was covered with loose, massive clast-supported pebbly sand and granules.

[27] Channel c1 correlates with channel c2. Together, they constituted a single right-deflecting channel that post-dated channel d. Our correlation is based on their lithologic similarity, their stratigraphic position and the similar elevations of their upper and lower contacts. Other evidence includes (1) the arrangement of and imbrications in the pebbly gravels in c1 were consistent with a right-curving channel course (Figure 5), as indicated by its thalweg (Figure 4c); and (2) it was consistent with the asymmetric widening of channel d on the right.

[28] Could the fault-bounded segment c2 be a channel fragment that was much older than c1 and just lodged within the fault zone near channel c1? In other words, are we correlating channel segments of different ages? We think this possibility is very remote. First, the outline of the channel and the deposits within it were still coherent, which suggests a relatively young age. Second, as will be shown later, the shapes and deposits of older channels to the northwest do not make them better candidates than c1 to be the downstream correlative of c2. In support of this correlation, it is worth reiterating that channel c merged with d right after it departed the fault zone. This proximity of the right deflection of channel c to the fault zone suggests that when channel c was incised, channel d was nearly connected with its former upstream segment. Perhaps, the

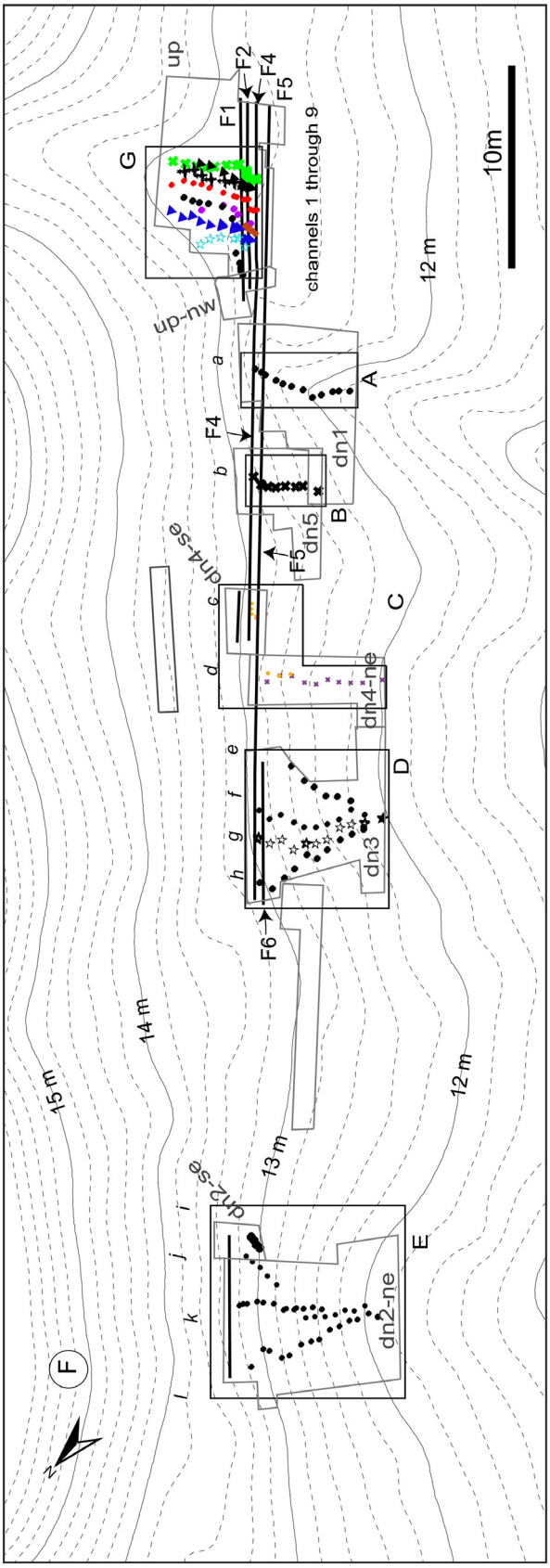


Figure 4. (continued)

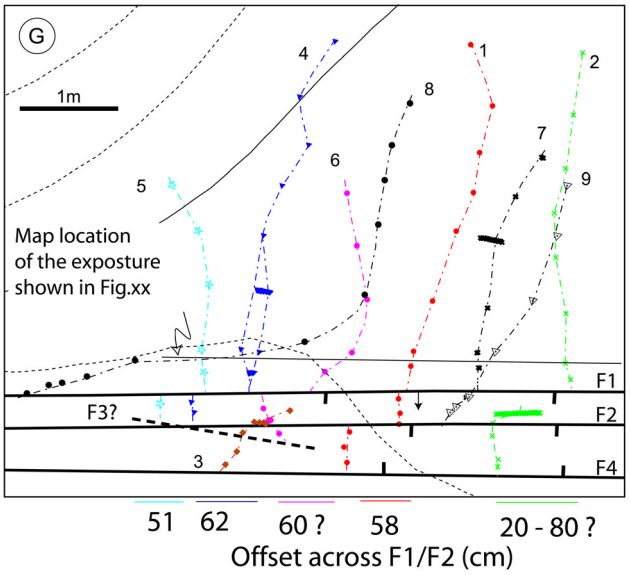


Figure 4. (continued)

rupture that immediately postdated formation of channel d offset the channel only a small amount, enabling a new channel connection to form between the upstream and downstream channels. If, for example, the offset were merely half the width of the channel, it would be relatively easy for water in the upstream channel find its way into the slightly offset downstream channel and to erode that portion of the fault zone between the channels. However, if the offset of channel d was much larger than the width of the channel, the connection would be more difficult to reestablish.

4.1.4. Channels e, f, g, and h

[29] The excavated volume 30 to 36 m northwest of the upstream source channel contained four channels, e, f, g and h, that fanned out upstream toward the fault zone (Figure 4f). Channels f and g trended roughly at right angles to the fault, whereas channels e and h merged from the right and left, respectively (Figure 4d). All four channels merged into a single channel 6 to 7 m downstream from the fault.

[30] Channel f was the deepest and widest of the four (Figure 4d). Its cross-sectional shape was roughly U-shaped. Locally, it had a secondary thalweg to the southeast, most likely the remnant of an earlier phase of downcutting. Channel h, another deep channel, had variable cross-sectional shape and stratigraphy. The cross-sectional shape of channel h changed dramatically from cut to cut. Note that in exposure ne10, immediately adjacent to the principal fault (F5), channel h had a steep northern bank and reclining southern bank. The asymmetry in channel shape suggests that channel h made a sharp turn to the southwest

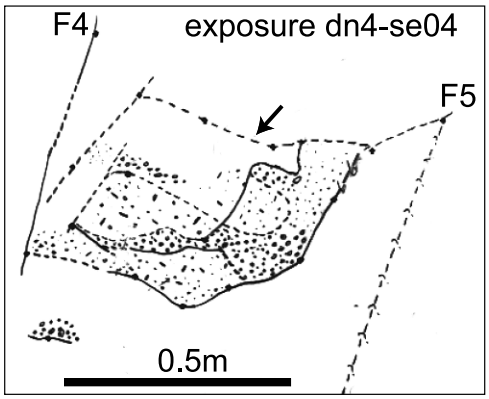


Figure 6. Map of exposure dn4-se04 shows the stratigraphy in channel c2.

as it departed the fault zone. Such a turn would be consistent with the trace of its thalweg indicated by the plot of thalwegs in cuts ne06 through ne09 in Figure 4d. Channel g was a shallow, less conspicuous channel between channels f and h. In cross section, it was narrow and contained channel sand and gravel of varying thickness at near its base. Channel e was also shallow. Channel e was still recognizable in exposure ne02, but it disappeared downstream, in ne01 and ne00. Channel e could not be traced with confidence upstream of ne07, closer than 2 to 3 m of the fault zone. One possibility is that bioturbation had obliterated the trace of channel e near the fault. Although we cannot rule out this possibility, it seems unlikely as no other channels, including much older ones, had been completely erased by bioturbation. Another possibility is that the headward limit of channel e was near exposure ne07 and that the channel was formed by headward erosion and that the channel did not reach or cross the fault zone. The longitudinal profile of channel e supports this hypothesis (Figure 7). From exposures ne07 to ne06, the profile exhibited a sharp drop in elevation and the width of the channel narrows (Figure 4d). Thus ne07 might slice across the knickpoint of channel e.

[31] Traces of thalwegs alone also suggested that channel f was the oldest of the four channels. Of the four channels, channel f occurred in the middle and perpendicular to the fault, flanked by channels h and e from left and right, respectively. Channels g and h were younger than f even though they appeared to be offset more than f from the source. The rationale behind the above speculation is that the upstream channels in this stretch of the San Andreas fault meet the fault almost orthogonally. This implies that downstream channels should also depart the fault perpendicularly, unless the microtopography near the fault (for example, an older downstream channel in close vicinity) favored a deflected channel course, e.g., channel h. Cross-

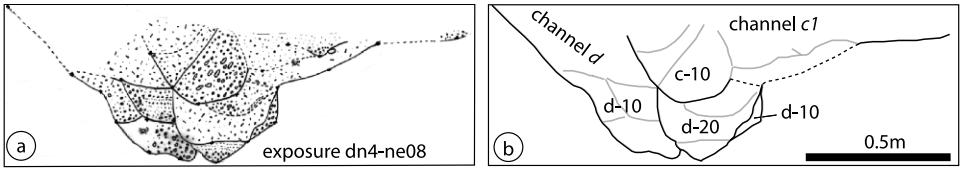


Figure 5. Stratigraphic units of channels d and c1, illustrated using exposure dn4-ne08.

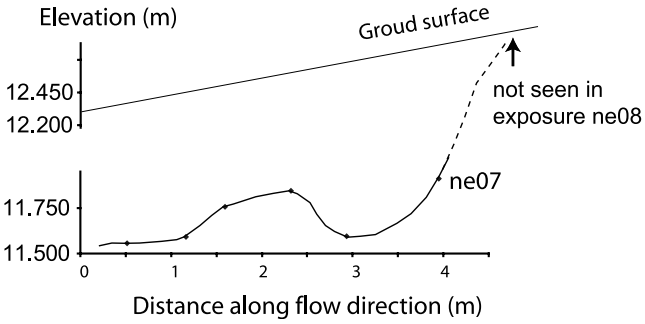


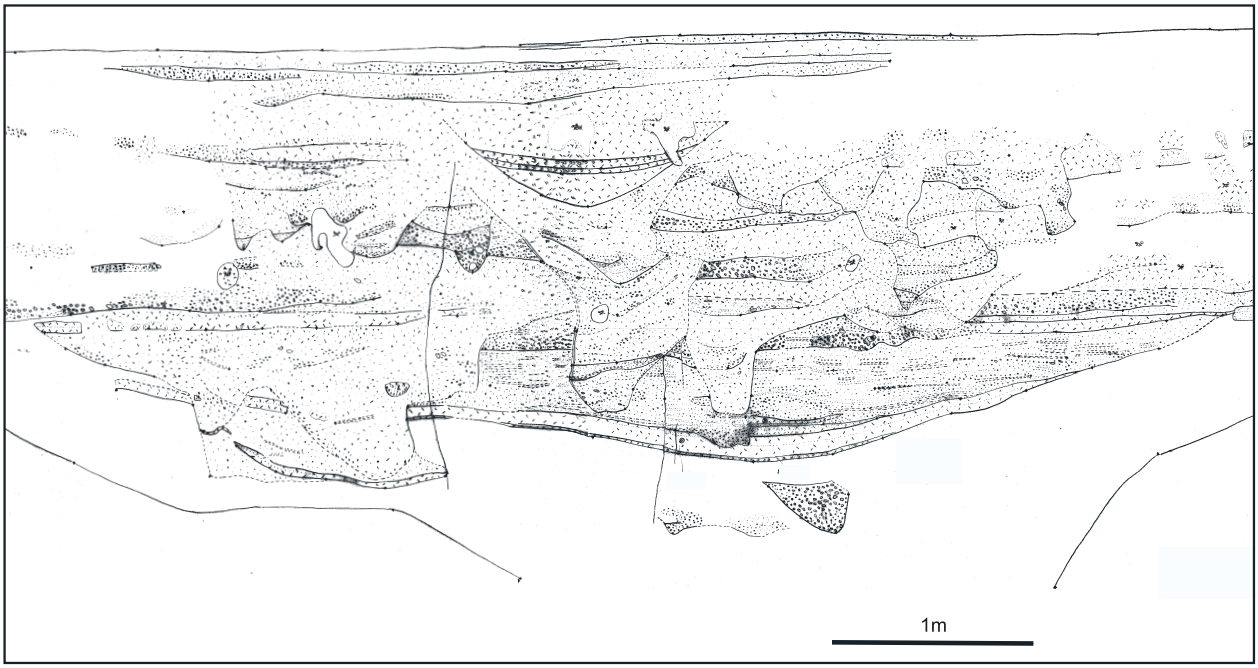
Figure 7. Longitudinal profile of the thalweg of channel e. The hollow in the profile just downstream from exposure ne07 suggests that channel e was eroding a plunge pool at this location and may not have eroded headward across the fault. If this is true, the channel cannot be used as an offset piercing line.

cutting relationships provided information about the relative ages of the channels (see Figure S3). Channel f was older than channel h, which was in turn older than channel g. The age of channel e relative to the ages of channels g and h was indeterminate, because channel e did not have direct contact with channels g or h. This left us with this temporal ordering: f > h > g and f > e.

4.1.5. Channels i, j, k, and l

[32] Another group of 4 channels existed farther northwest channel h (Figure 4f). An unnamed trench cut parallel to the fault confirmed that no channels existed downstream from the fault between this group of four channels and channel h.

[33] Channel k was the largest and deepest channel in the volume and intersected the fault at nearly a right angle (Figures 4e and 4f). Channel l, another deep channel, exited the fault zone at an acute angle and snaked



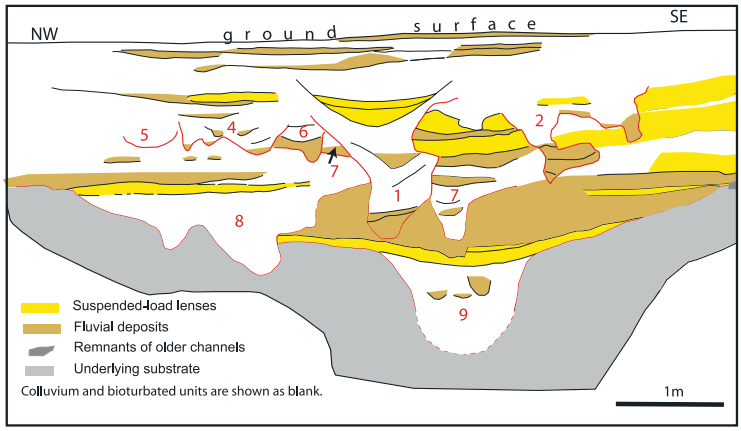


Figure 8. (a) Map and (b) simplified map of the wall of an excavation upstream from the fault show eight of the nine nested upstream channels. Suspended load silts (in yellow) testify to the temporary ponding of the drainages behind shutter ridges. Channel margins and names are in red. View is upstream.

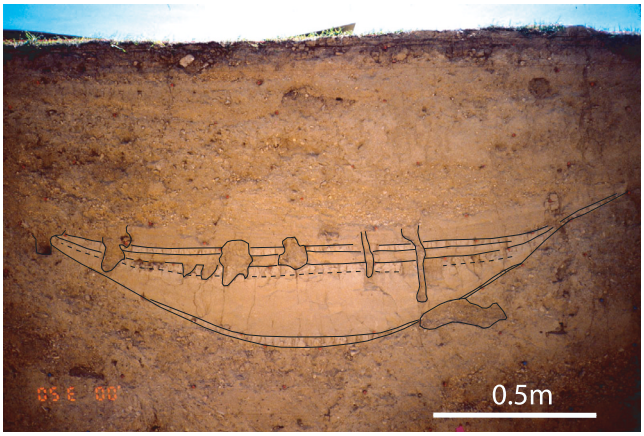


Figure 9. Photograph of the suspended load lens in channel 1. Note that the lens has a gently curved top and deeply curved base and consists of multiple individual lenses. Each of the lenses is thickest in the middle and thins to feather edges on their margins. The lenses consist of fines deposited out of suspension in a muddy puddle just upstream from the fault and straddling the middle of the channel. The photo is flipped so that the viewing direction is upstream.

downstream (Figure 4e). It had an irregular channel floor with multiple thalwegs, separated by lateral ridges. The configurations of channels k and l suggested that k was older than l. Channel k left the fault at nearly a right angle and continued downstream in a nearly straight path. Furthermore, the channel thalweg run immediately below the lowest point in the topographically visible channel (Figure 4f). Channel l, by contrast, flowed in the center of the topographic channel only in its lower reaches and entered the topographic channel from a position well up on the northwestern flank of the topographic channel. This suggests that it was diverted left-laterally into the channel. Thus channel geometries suggests that channel l postdated channel k. Our exposures of stratigraphic relationships confirmed this relationship. Figure 4e (also see Figure S4) shows that channel l truncated the northern bank of channel k in exposure ne08 and its thalweg a few meters farther downstream, between ne05 and ne04. Downstream from ne04, channel k was completely absent, having been completely obliterated by channel l. Thus channel k was reoccupied and erased by the younger channel l at this juncture.

[34] Channel j intersected the fault zone at a 45° angle (Figure 4f). It flowed westward, away from the fault zone and merged with channel l about 7 m downstream. The channel was well expressed up to a few tens of centimeters from the fault, typically marked by a thin lens of sandy gravel. Farther downstream, channel j cut into the upper colluvial fill of channel k, and then it continued northwestward and merged with channel l. This correlation implies that channel j was younger than both channels k and l. Channel i lay just a meter or so south of and run almost parallel to channel j (Figure 4e). In the southernmost exposure of channel i (ne11), it was well defined as a 60-cm-wide lens of sand and fine gravel [*Liu*, 2003]. Further downstream, channel i was not visible, probably due to a lack of coarse fluvial channel fill. The relative age of channels i and j was indeterminate, because no direct crosscutting relationship was exposed.

4.2. Upstream Channels

[35] The subsurface stratigraphy of the outlet of this drainage, just upstream from the San Andreas fault, differed greatly from that downstream. Whereas 12 downstream channels string out separately along a 55-m length of the fault, 9 upstream channels nested at the outlet of the drainage (Figure 4f) This nesting represents repeated cuts and fills in roughly the same place.

[36] Figure 8 illustrates the basic nature of the nested upstream channels, using the map of exposure up-sw06, whose map position is indicated on Figure 4g. Eight of the 9 upstream channels were visible in this cut. The base of the deposit of these young channels was easy to recognize, because the underlying late Pleistocene deposits were massive and featureless fine-grained sand and silt with sparse gravel lenses. Bioturbation had homogenized the late Pleistocene substrate, and pedogenic carbonate precipitation had given it a pale hue and induration that contrasted sharply with the richer shades and looser consolidation of the recent channel deposits. In general, the boundaries of individual channels were also easy to recognize.

[37] A prominent feature of many of the channels was a distinctive lens of well-sorted fine sand to silt. These beds are highlighted in yellow in Figure 8. Such beds were absent from any of the downstream channels. Figure 9 is a photograph of one of the lenses. The lenses consisted of fines deposited from suspension in a

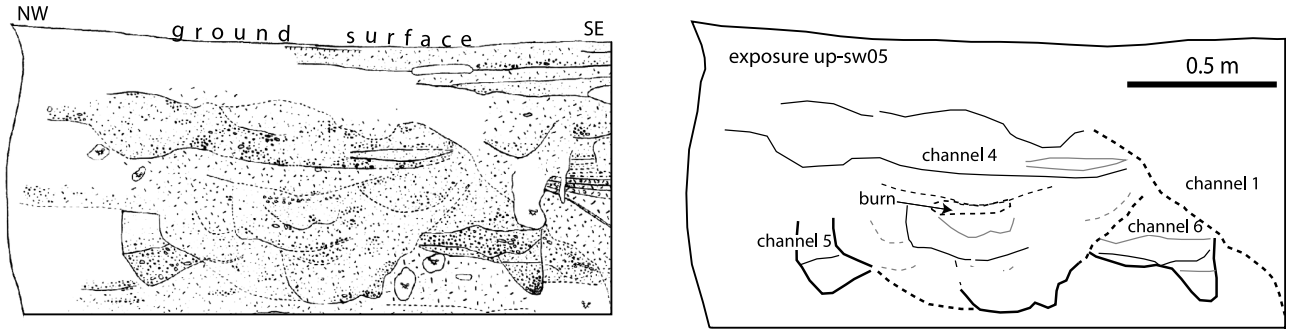


Figure 10. Stratigraphic units of channels 4, 5, and 6, illustrated using exposure up-sw06. The stratigraphy in channel 4 was grouped into five major units.

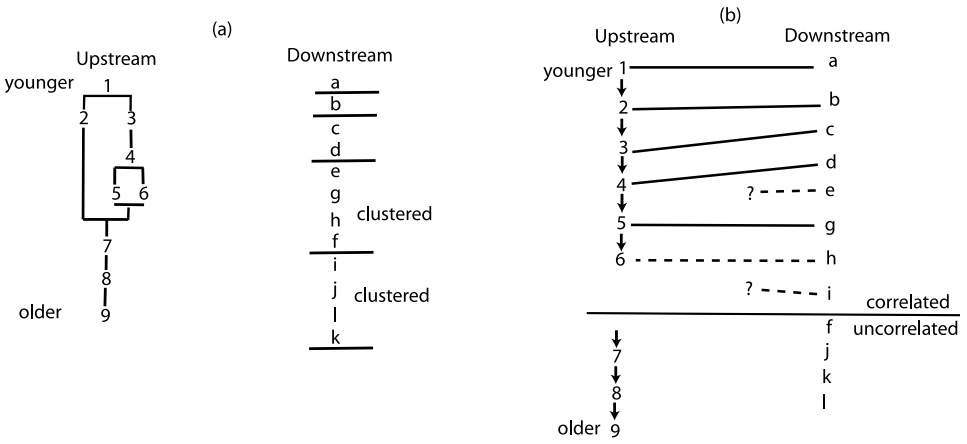


Figure 11. (a) Relative ages of upstream and downstream channels. The sequence of the upstream channels is based on crosscutting relationships. Ambiguities appear as bifurcations. On the downstream side, age is assumed to increase with the distance from the upstream trench, with a couple of exceptions that are constrained by stratigraphic relationships. (b) Correlation of upstream and downstream channels. Solid lines designate confident correlations. Dashed lines indicate uncertainty.

muddy puddle just upstream from the fault and straddling the middle of the channel. They appeared to be the result of blockage of the channel by a shutter ridge, emplaced by large dextral offset along the fault. Thus the silty lenses likely are direct evidence of occasional large ruptures of the fault.

[38] Crosscutting relationships among the channels revealed the sequence of their formation, from 1 to 9, from the youngest to oldest. Some of these relationships were ambiguous in Figure 8. For instance, the relationship between channels 5 and 6 was ambiguous, because the two channels had no direct contact. In such cases, to determine relative ages used other evidence, which we discuss in the following sections.

4.2.1. Channels 1 and 2

[39] Channel 1 sat in the middle of the exposures and was 1.8 m deep (Figure 8). Channel 2 rested a meter or so southeast of channel 1. The principal characteristic of channel 2 was its narrowness. In many of the exposures, it was more than a meter deep but only ten or twenty centimeters wide. The channel geometry was complicated by a second, higher side channel, which merged with the main channel before the channel entered the fault zone. In plan view (Figure 4g), both channels intersected the fault zone at a high angle. They were completely cut off by F4. Crossing F4, we immediately ran into a wall of indurated pebbly sand and silt with a pedogenic carbonate horizon (B_k), similar to the substrate exposed in all downstream trenches.

4.2.2. Channels 3, 4, 5, and 6

[40] Channels 3, 4, 5, and 6 appeared in the northwestern part of the excavated upstream volume. All four were shallow channels at a depth of 1 to 1.2 m below the ground surface (Figures 8 and 10).

[41] Channel 3 was unlike the other channels upstream from the fault, in that it did not exist upstream from the fault zone. It was only about a meter long, existed only within the fault zone and trended westward, rather than southwestward (Figure 4g). If it extended farther upstream, it had been eroded away by the younger channel 1. Channel 3 was demonstrably younger than channels 4, 5 and 6, because it was not offset by fault F3, and because it cut channels 4 and 6 in exposures up-sw08, up-sw09, and up-sw10 (Figure S8). Channel 4 had a W-shaped to nearly square-shaped cross section. It was due to two major phases of down-cutting that reached to similar depths (Figure 10). Channel 5 was a small channel whose upper section was eroded away by scouring of channel 4. It was narrow with a semicircular floor in most exposures. The preserved portion of channel 5 commonly contained two packets of fluvial sediments. In up-sw06 (Figure 10), the lower of the two beds was massive and coarser-grained, composed of pebbles in a matrix of granules to coarse sand. The upper bed was finer-grained, well-sorted coarse to medium sand. The sorting of both of these beds indicates they were fluvial deposits. Channel 6 was truncated by channel 4 on the northwest and by channel 1 on the southeast. Only the lowest 40 cm of the channel was preserved. The surviving portion of channel 6 was preserved best in exposure up-sw05 (Figure 10). There it was filled with two well-sorted fluvial beds separated by a thin layer of poorly sorted granule-rich silty sand. The lower fluvial layer consisted of loose pebbly granule-rich sand that fined upward slightly. The upper fluvial bed was coarser-grained, and it was deposited when the channel floor was flat and wider.

[42] In plan view (Figure 4g), channels 4, 5, and 6 were subparallel and moderately sinuous. They were sharply offset a similar amount by fault F1. Also, they disappeared about 0.5 m north of the main strand F4. Because of this disappearance before the main fault strand, we suspected that they were offset by another strand, F3. In the reach between F1 and F3, channels 4 and 5 remained straight, whereas channel 6 flowed southward.

4.2.3. Channels 7, 8, and 9

[43] In a typical upstream cut, channels 7, 8, and 9 occupied the lower two thirds of the exposure (Figure 8). The stratigraphy of all three channels was easily correlated from exposure to exposure. Commonly in channels 7, 8 and 9, the silty fine sand lenses that represented the

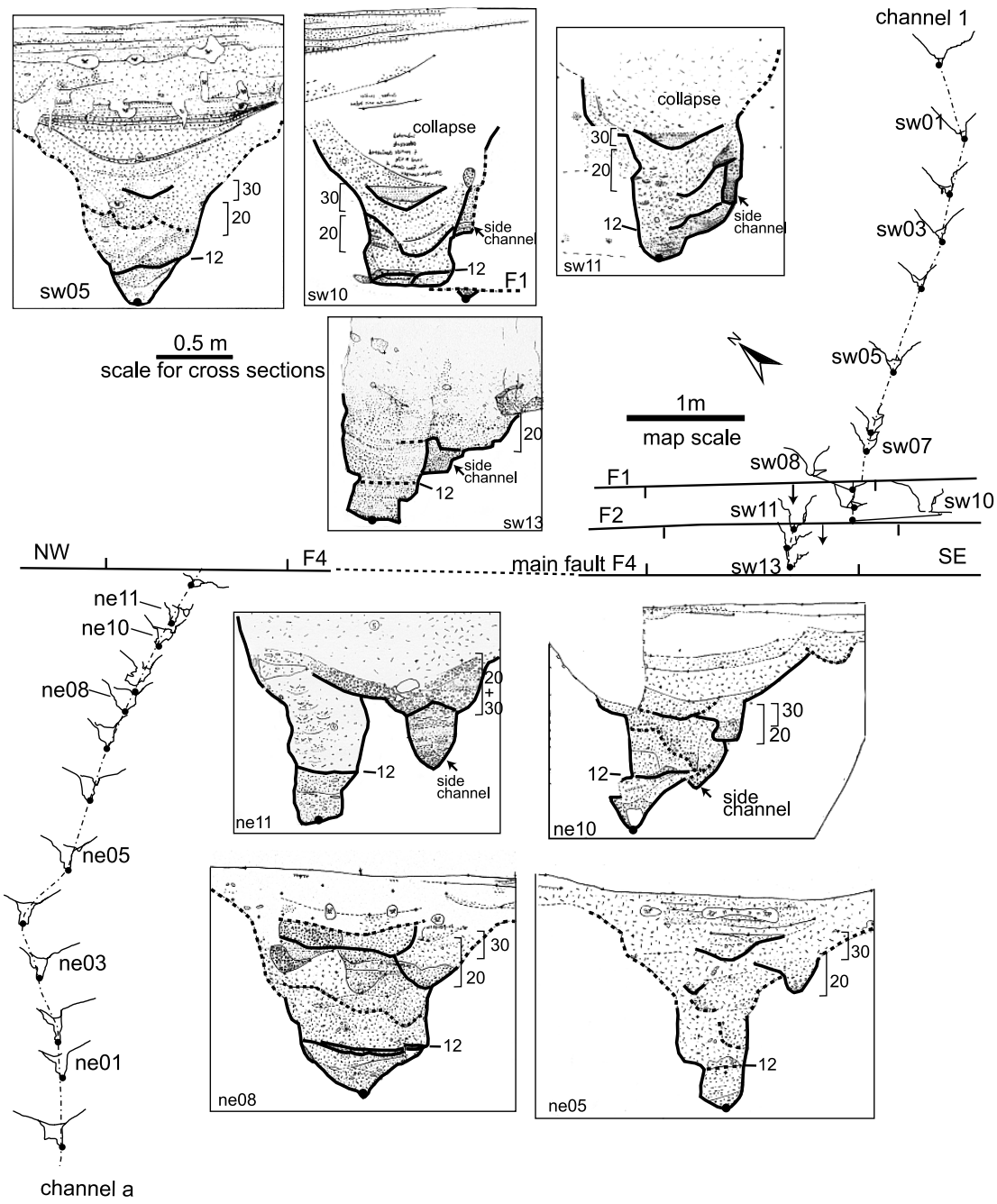


Figure 12. Correlation of channel 1-a based on the similarity of stratigraphy and morphology in channels 1 and a. The eight vertical exposures show examples of the stratigraphic details within the channels. In map view, the dots indicate the geographic position of the deepest channel thalweg. Outlines of the channel shape and key internal contacts allow viewing the changes in the features along the trend of the channel. Note that the scale of the detailed cross sections is larger than that of the map.

behind-the-shutter-ridge deposits were broader than in younger channels. Two suspended load beds that topped channel 7 were the widest. These beds overlaid the central channel and extended over prechannel 7 colluvial apron up to 5 m farther southeast. They might have also extended to the northwest, but if so, they had been removed by erosion during the creation of younger channels. The width and height of these beds suggested that the shutter ridge was high at the time of the deposition of the lenses. This could either be due to a considerable amount of vertical motion along the fault with downstream side moving up, or a juxtaposition of a broad topographic high downstream with channel 7, or a combination of the two. Detailed descriptions of the strata in channels 7, 8 and 9 were given by *Liu* [2003] (chapter 2, section 2.3.3.6).

[44] In plan view (Figure 4g), channels 7 and 9 met the fault zone at a high angle. The path of channel 8 is different. It veered sharply to the northwest, less than a meter upstream from the fault. It then flowed parallel to the fault

before being truncated by fault F1 at the northwestern edge of the excavated volume.

5. Channel Correlation

5.1. General Criteria for Channel Correlation

[45] Multiple criteria were available for assessing correlations. Channel morphology and stratigraphy described in the section above are important information to match channels across the fault. In addition, three other considerations are important in making bona fide correlations. These are (1) the relative ages of channels on each side of the fault, (2) the similarity of the angles at which channels enter and exit the fault, and (3) age constraints from ^{14}C dates on charcoal extracted from channel strata. We use all five criteria in proposing correlations, below.

[46] We begin by ordering the relative ages of channels on each side of the fault (Figure 11a). On the upstream side of the fault, the relative ages of many of the channels were clear from their crosscutting relationships. On the downstream side of the fault, the order of formation of the channels may be inferred from their distance from the nearest upstream channel and, where available, their crosscutting relationships. This criterion would, of course, be inappropriate for any channel that originated from upstream channels farther to the southeast. Furthermore, in matching of upstream and downstream channels, it is a necessary but not a sufficient condition that these relative ages be obeyed. Figure 11a illustrates a problem that arises immediately upon showing this hypothetical ordering of upstream and downstream channels: the downstream side had three more channels than the upstream side. Plausible explanations for this mismatch include that upstream channels had been obliterated by the incision of younger channels, or the downstream sequence contains channels that did not originate from the upstream channel, or both.

5.2. Channel 1-a

[47] Three lines of evidence support the correlation of channel 1-a. First, channel 1 was the youngest channel on the upstream side, and channel a was the closest of all the downstream channels to the upstream channel.

[48] Second, the shapes of the channels were similar. However, in considering the match of channel shapes across the fault, we must first evaluate how similar channel shapes need to be in order to be plausibly correlated across the fault. Generally, the variations in channel shape along profile were large. Only the principal characteristics of the channel continued from one exposure to the next. These were the basic V-shaped geometry of the channel and its depth. Second-order features, such as overhangs and other details of the channel walls, commonly were not continuous from exposure to exposure. Thus we should require only that the first-order characteristics correlate across the fault. The shapes of channels 1 and a were quite similar immediately upstream and downstream from the fault. In downstream exposure ne11, channel a was about 2 m deep and consisted of a deeper and a shallower channel, separated by an uneroded septum (Figure 12). The deeper channel had a nearly flat base, about 40 cm across. In upstream exposure sw13, channel 1 consisted of only one channel. However, like channel a it was about 2 m deep. Channel 1 was also asymmetric, with a steep and a shallow wall. This asymmetry would be very similar to the shape of channel a in exposure ne11, if one removed the septum between the principal and auxiliary channels in channel a. Without this septum channel a would have the same asymmetry as channel 1, steep on the northwest and shallow on the southeast.

[49] A close inspection of the internal stratigraphy of the upstream and downstream channels supports this interpretation, because it shows that the smaller channel had longitudinal continuity. Close to the fault (in exposures sw10 through sw13), this "side channel" cut to the southeast and was plastered onto the southeast wall of the older main channel (Figure 12). Downstream from the fault, the channel remained on the southeast side of the main channel from exposures ne11 through ne09, and merged into the main channel in the rest downstream exposures. The correlation of channels 1 and a is supported by other details of the stratigraphy within the channels, as well. In particular, units 12 and 30 were comparable. Unit 12 was a diagnostic thin bed of laminated fine sand to silt that mantled the underlying basal deposits of both channels (compare exposures sw05 and ne08; Figure 12). It occurred in most upstream and downstream exposures. Unit 30 was the bed immediately predated the offset event. It consisted of two well-sorted fluvial layers, which formed an inversely graded sequence; the lower bed was finer grain sized than the upper one. It was continuously correlative among most exposures.

5.3. Channel 2-b

[50] Of all our proposed correlations, the match of channels 2 and b is the strongest. The strength of the correlation lies in the similarity of their channel shapes and internal stratigraphy. Figure 13 displays the outlines of the two channels. The shapes of both channels b and 2 were about 1.5 m deep and very narrow. These two channels had, in fact, the lowest width-to-depth ratio of all the channels at the site. A side channel in the upper reach of the channel 2 merged with the main channel just upstream from the fault zone. Thus the shape of channel 2 in its lower reach was as simple as that of channel b. The strata within channels 2 and b also correlate exceptionally well. Both channels had four characteristic units, 10, 20, 30 and 40. Among these, unit 20 was the most diagnostic. This upward fining sequence comprised horizontally bedded thin layers of framework-supported pebbles and sand. Within each layer, the sediments were remarkably well sorted.

[51] Recall that from the crosscutting relationships in the upstream exposures, one cannot determine whether channel 2 was older or younger than channel 3 (Figure 11a). From the correlation between downstream channel b and channel 2, we can now say that, in fact, channel 2 was younger than channel 3.

5.4. Channels 3-c and 4-d

[52] On the basis of crosscutting relationships and the match of channel 2-b, channels 3 and 4 were the third and fourth oldest channels upstream from the fault. Similarly, channels c and d were the third and fourth oldest channels downstream from the fault.

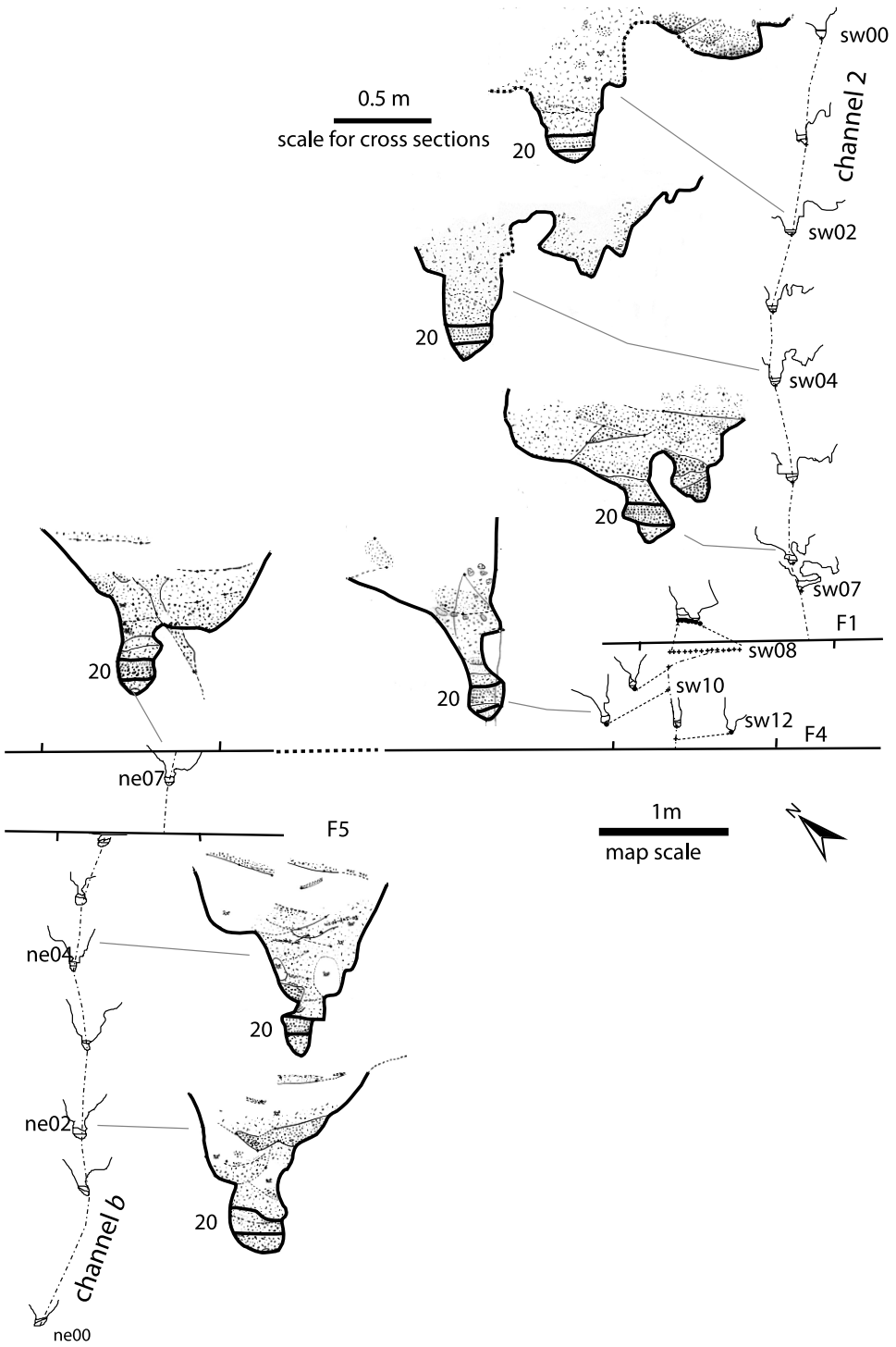


Figure 13. Correlation of channels 2 and b. The unusual narrowness of channels 2 and b and the similarity of their internal stratigraphy provide definitive evidence for their correlation. The dotted portion of the fault indicates much of the fault length between the upstream and downstream segments was removed to enable presentation of the comparison on a single page. Note the different scales for map and cross sections.

[53] The similarity of channels 4 and d strongly suggests that they are correlative (Figure 14). The morphologic features common to both channels include their W-shaped channel profile, their large width/depth ratio, their 1.2-m depth beneath the surface near the fault zone, and the fact that they both approached the fault at nearly right angles. Furthermore, both upstream and downstream channels experienced two cut-and-fill episodes. On both sides of the fault, the second down-cutting reached as deep as the first phase and widened the channels by scouring the

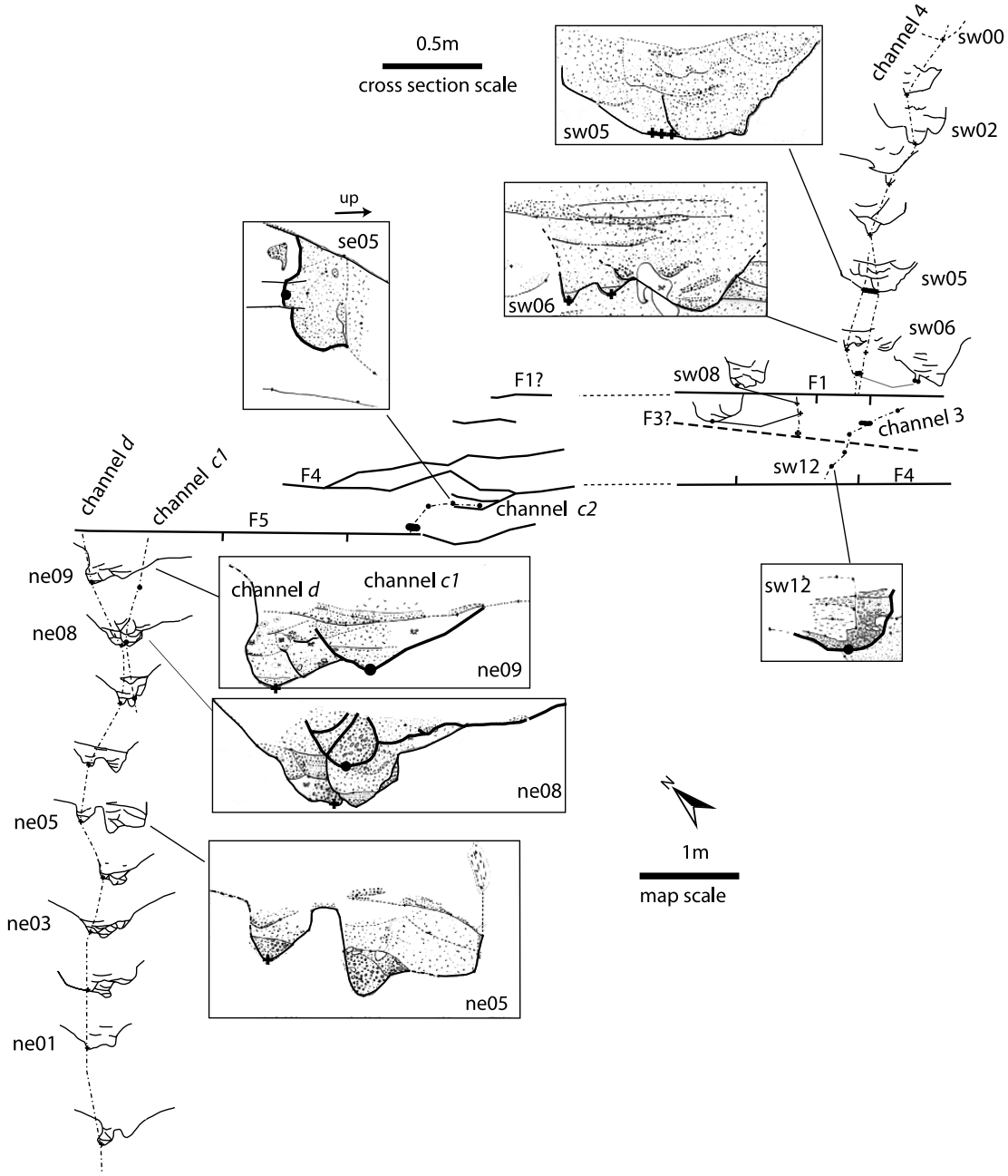


Figure 14. Map and cross sections of channels 4 and d illustrating the basis for correlation of these two channels. The correlation is strongly suggested by the W-shaped channel profiles of both upstream and downstream segments and the similarity of their stratigraphic sequences. This match is also consistent with the match of the deflected channels 3 and c.

southeastern bank. The deposits within channels 4 and d are also similar. Sediment within both channels was predominately massive, poorly sorted sandy, pebbly debris. The only fluvial units within this colluvial debris were thin basal wisps of granule- and pebble-dominated fluvial deposits above each of the basal channel scours.

[54] Having established a likely correlation between channels 4 and d, we can now consider plausible upstream correlations of channel c. Channel c consisted of two parts (section 4.1.3) Channel c1 was superimposed on channel d downstream from the fault zone but diverged eastward away from channel d near the fault (Figure 14). Channel c2 was within and parallel to the fault zone, just a few meters to the southeast. The salient question, now, is whether channel c2 is correlative with upstream channel 3. The stratigraphic position of channel 3 is proper for such a correlation, since it was demonstrably younger than channel 4 (section 4.2.2). Secondly, the fact that both channel c2 and channel 3 ran nearly parallel to the fault and within the fault zone also supports the correlation. In addition, channels 3 and c2 had similar shapes; both had a clear, circular channel profile. Strata within both channels varied greatly along profile, so we cannot martial this as strong evidence for correlation. Nonetheless, in both

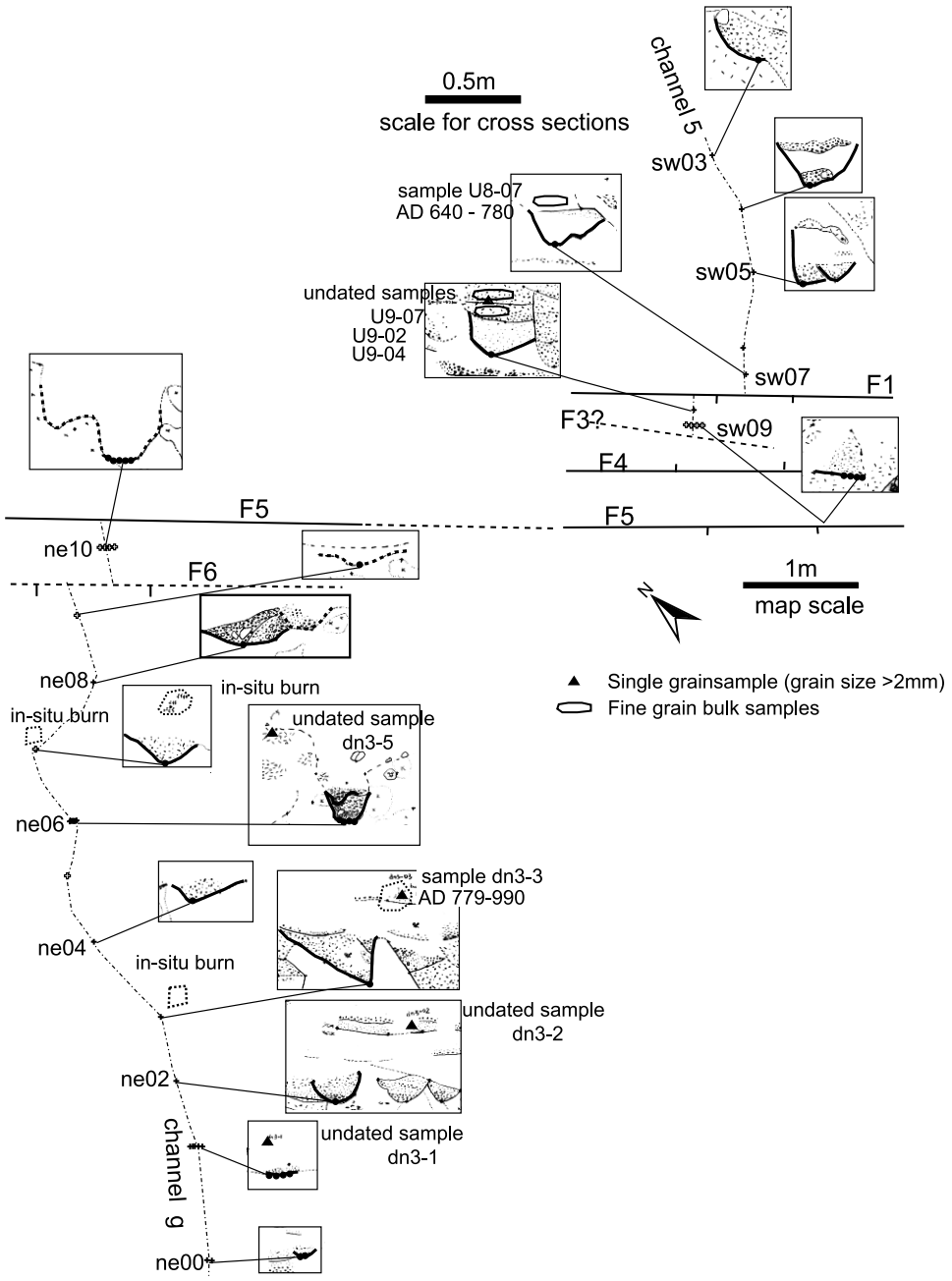


Figure 15. Summary of evidence for the correlation of channels 5 and g. Their size and stratigraphy are similar. The similar ages of two radiocarbon samples from the two channels also support the correlation. Open symbols for channel thalwegs indicate that the locations of the channel at these exposures are estimated. In particular, in exposures ne09 and ne10, the channel did not have any distinctive well-sorted coarse-grained layers and was barely recognizable by slight color contrast between channel-filling colluvium and bioturbated alluvium. Hence the positions of channel g in these two exposures were conjectural.

channels the thickness of the strata was about 30 cm in exposures near the fault.

5.5. Channel 5-g

[55] The next correlation of upstream and downstream channels is more difficult to make, because of ambiguities in the relative ages of channels both upstream and downstream from the fault. Upstream channels 5 and 6 antedated channel 4, but there were no crosscutting relationships to tell which was the younger of the two. Downstream channels e, f, g, and h were nested together (Figure 4d), with a temporal ordering of f > h > g and f > e. Channel e probably did not reach the fault, so we would not expect to be able to find a match for it across the fault. Even if channel e did reach the fault, the angle it left the fault zone is not compatible with either channel 5 or channel 6.

[56] The best match is between channel g and channel 5 (Figure 15). The basis for this proposed match is channel

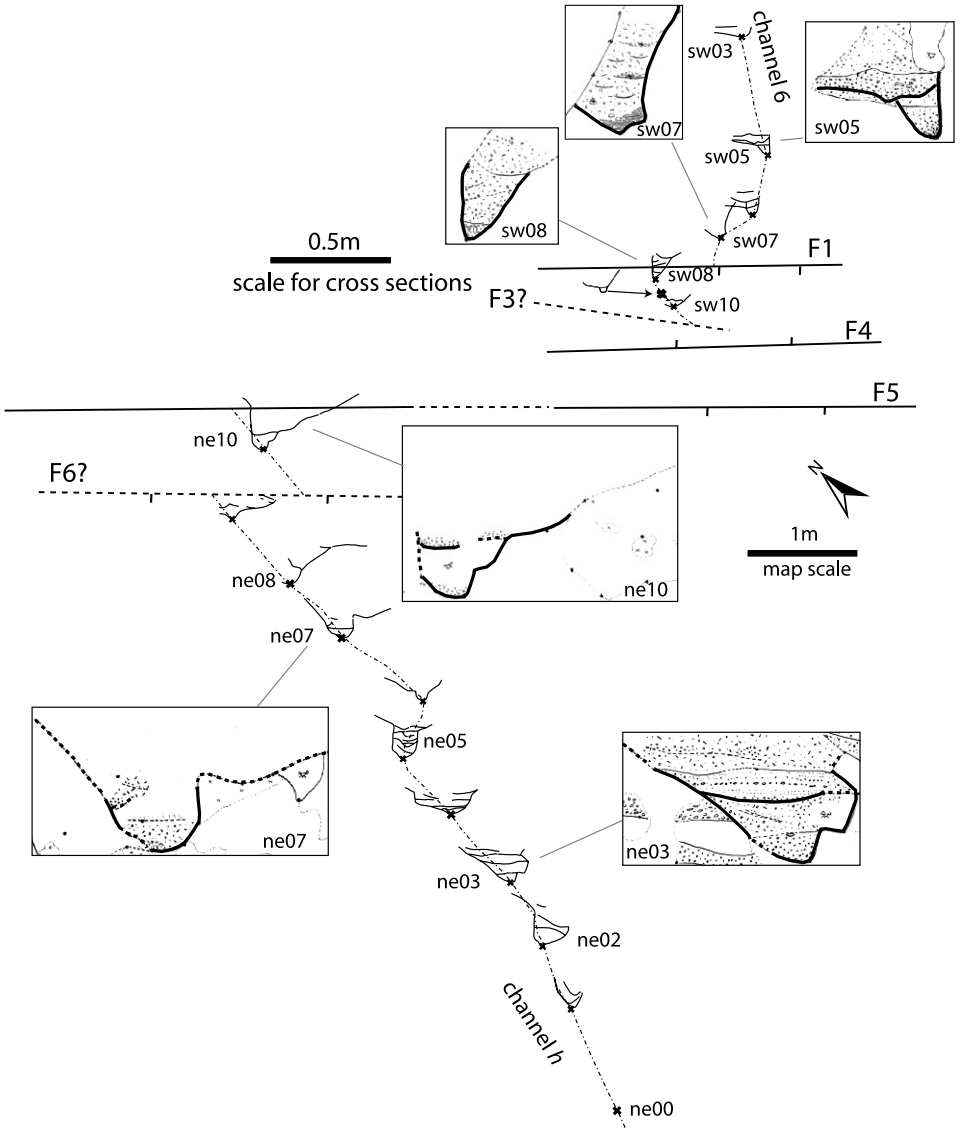


Figure 16. Correlation of channels 6 and b. The evidence includes their similar southward flow directions. Their internal stratigraphy is also similar.

geometry, stratigraphy and datable carbon in both channel segments. Both channels were narrow and shallow in mappable channel stratigraphy ($\leq$40 cm wide and $\leq$40 cm deep). Unlike channel 6, both were roughly as wide as they were deep and were relatively flat bottomed. Their stratigraphy was similar: predominantly well-sorted fluvial sands with sparse pebbles, overlain by poorly sorted sandy colluvium. In neither channel was there a consistent record of multiple incisions and aggradations. Further support for the correlation of channels 5 and g is the presence of charcoal in both channels. We will discuss the radiocarbon ages of these samples in more detail later, along with ages determined for other samples at the site. For now, let it suffice to say that samples from both channels yielded similar ^{14}C ages.

5.6. Tentative Correlation of Channel 6-h

[57] Erosion of much of channel 6 by younger upstream channels makes matching of this channel a special challenge and less certain. Nonetheless, the correlation we suggest is the most plausible one. The bases for correlation are the channel size, fill and its orientation.

[58] The angle of intersection of channel 6 with the fault is the strongest basis for correlation (Figure 16). Channel 6 approached the fault zone at a distinctly acute angle. It was, in fact, the only upstream channel to trend southward as it approached the fault. We might expect, then, that its downstream equivalent would also trend southward away from the fault. Of all the downstream channels, only channels h and l had flow directions near the fault that were compatible with the deflection of channel 6. However, channel l was an unlikely match, because it was much deeper and wider than channel 6. It also had a more complex sequence of cut and fills and a more complex cross-sectional profile (Figure 4e).The general resemblance of the stratigraphy within the channels also favors correlation of channels 6 and h. Both channels had two well-sorted gravely to sandy fluvial beds near their base, separated by a

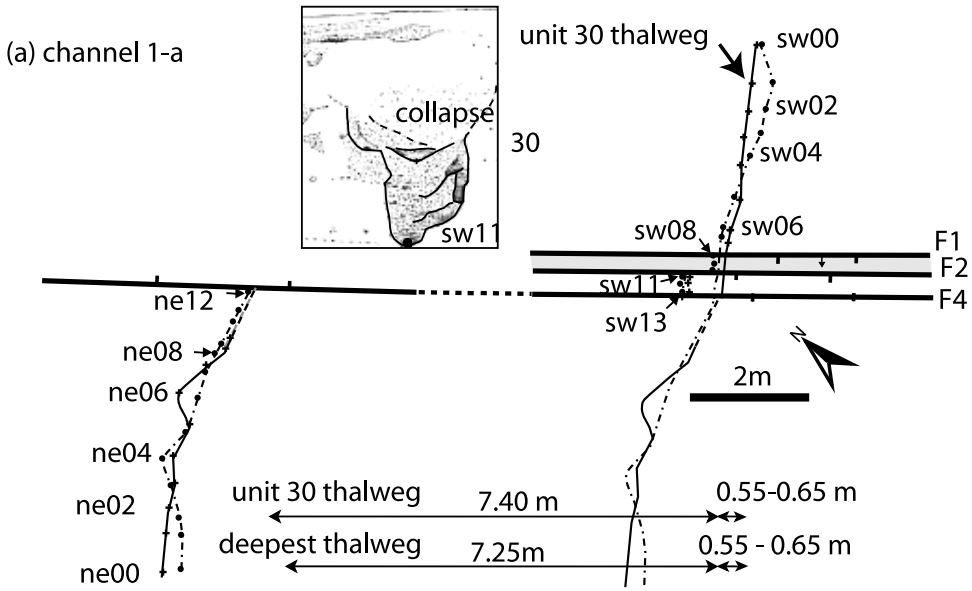


Figure 17. Horizontal and vertical offsets of the six channel pairs. (a) Offset of channel 1-a. The dextral offset of 7.8–8.0 m is indicated by the deepest thalweg and the base of unit 30. Most of this (7.25–7.42 m) is across the major strand, fault F4. (b) Total offset of channel 2-b. It is constrained to be 15.1–15.8 m by the deepest thalweg. Possible warping is confined to the reach immediately downstream from fault F5 and is about 0.4 m. (c) Restorations of channels 3-c requiring a total right-lateral offset of 20.7 ± 0.15 m. The majority of the offset is accommodated in the 0.8-m-wide zone between faults F3 and F5. (d) The 22.0 ± 0.2 m offset of channel 4-d, indicated by the average trend (dashed lines) of channel 4-d thalweg. The uncertainty is half the amplitude of channel meanders. Direct connection of channel thalweg suggests a slightly larger offset but within the uncertainty bound of that of the average trend. (e) Map showing the 30.0 ± 0.3 m offset of channel 5-g. Direct connection of data points suggests an offset larger than, but within the uncertainty bound of, that of the average trend. Open symbols for channel thalwegs indicate that the locations of the channel are uncertain at those exposures. (f) The 35.4 ± 0.3 m offset of channel 6-h, using a straight-line extrapolation. The 0.3-m uncertainty is half the maximum amplitude of channel meanders. The obliquity with which this channel intersects the fault zone suggests the offset could be substantially more than 35.4 m. (g) Vertical offsets of the six channel pairs. Longitudinal profiles of the two piercing lines of channel 1 delineate a graben within the fault zone, but the overall vertical offset across the entire fault zone is 5 cm, downstream side up. The vertical offset of channel 2 across the fault zone is 7–14 cm, downstream side down. The long profile of channel 3-c shows that the block between faults F4 and F5 is a small horst with little, if any, vertical offset across the faults. Yet, the total net vertical offset of channel 3-c should also include the offset across F1, which is 10 ± 5 cm, downstream side down. The irregularity of the long profile of channel 4-d suggests warping. However, the cumulative vertical offset across the fault since its incision is nil. Vertical offset of channel 5-g is relatively ill-constrained. If we use the trend of upstream points in the profile, the net vertical offset is 25–45 cm, with downstream side up. If we use a moderate river gradient, e.g., 3.24°, instead, the offset is 0–8 cm, downstream side down. The net vertical offset of channel 6-h is also ill-constrained. The upper bound of net vertical offset is probably about 5–30 cm, up on the downstream side. The lower bound can be 25 cm, down on the downstream side.

poorly sorted 25-cm-thick colluvial deposit (cf. exposures sw05, ne10 and ne03; Figure 16).

5.7. Uncorrelated Older Channels

[59] Thus far, we have made plausible correlations between 6 sets of upstream and downstream channels (Figure 11b). Three upstream channels, 7, 8 and 9, remain to be matched with downstream channels. Five downstream channels remain unmatched, e, f, i, j, k and l. None of these channels appear to match across the fault. The correlatives of channels 7, 8 and 9 must lie further to the northwest. The upstream correlatives of the unmatched downstream channels are slightly more complicated. They could have been eroded away by the younger channels, i.e., channels 1 through 6, or they may exist farther to the southeast, outside the bounds of the excavations.

6. Measurement of Offsets

[60] Now, we can measure the offsets of the 6 pairs of matched channels. The offset of each pair represents the cumulative displacement since the abandonment of the channel. We will mainly use the deepest thalwegs of channels as offset piercing lines. We are able to measure both horizontal and vertical offsets, because 3-D excavations and surveying by Total Station enable us to reconstruct

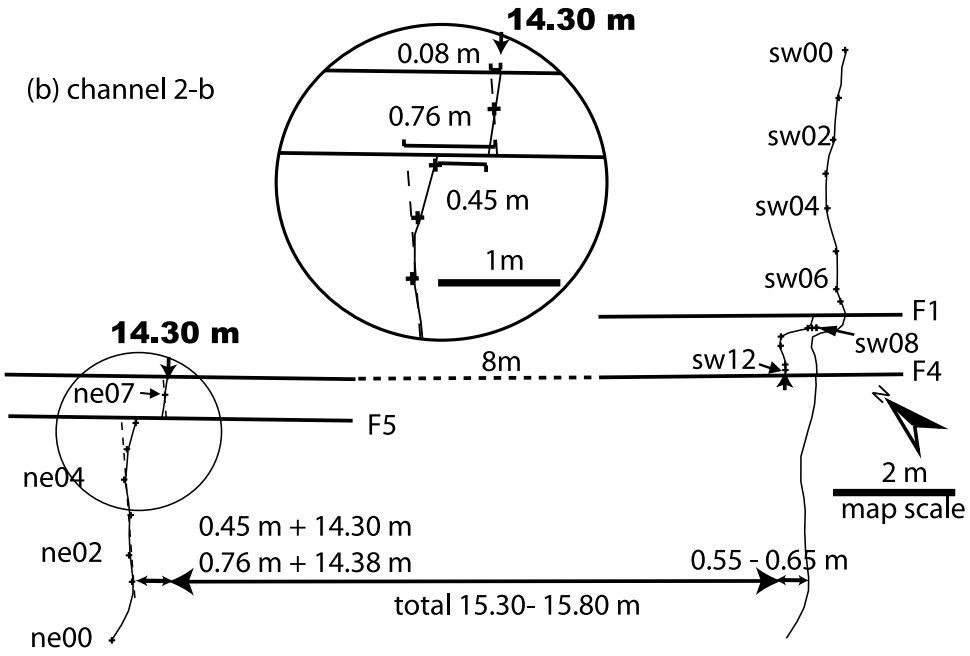


Figure 17. (continued)

the channel geometries in three dimensions. The precision of the measurements is on the order of 10 cm and is about what can be achieved measuring the offsets of a natural feature immediately after an earthquake.

[61] Faulting was concentrated in a zone just 1.5 to 2 m wide. This zone comprised six principal fault planes, fault F1 through F6 (Figure 4f). We did not find secondary traces outside this narrow zone within the channel stratigraphy. However, the total width of the fault zone in the substrate was larger than that is indicated by channels. The main fault zone in these older units was at least 4 to 5 m wide, judging from the extent of shear fabric within the substrate.

6.1. Minor Offset on Faults F1 and F2

[62] F1 was a shallow branch of F2. It was connected with F2 by a subhorizontal ramp ~1.8 m below the ground

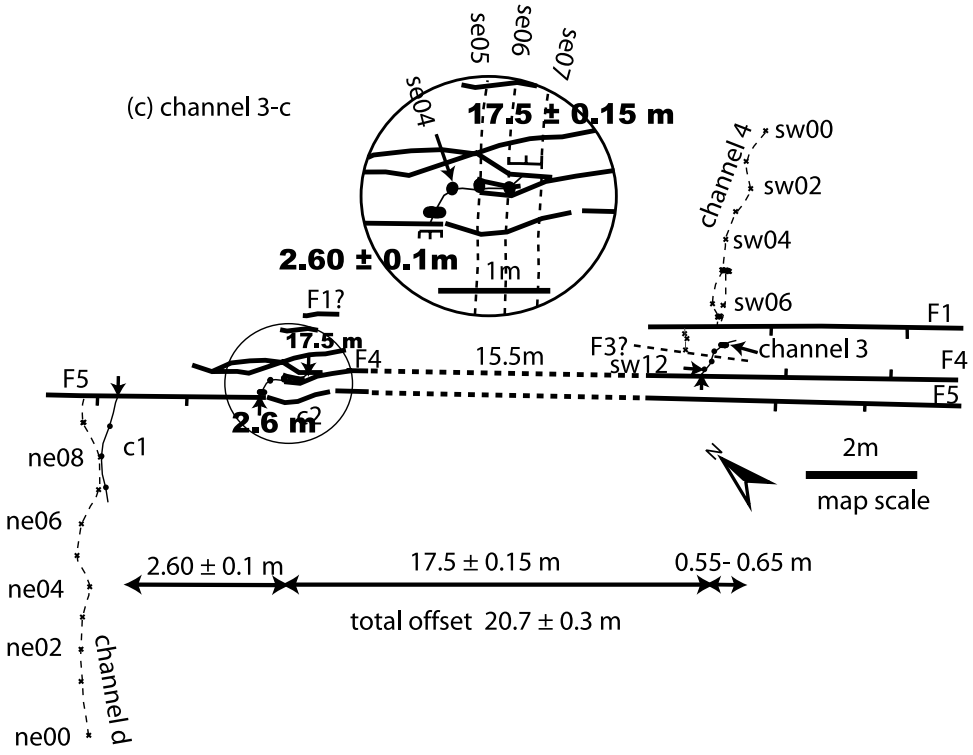


Figure 17. (continued)

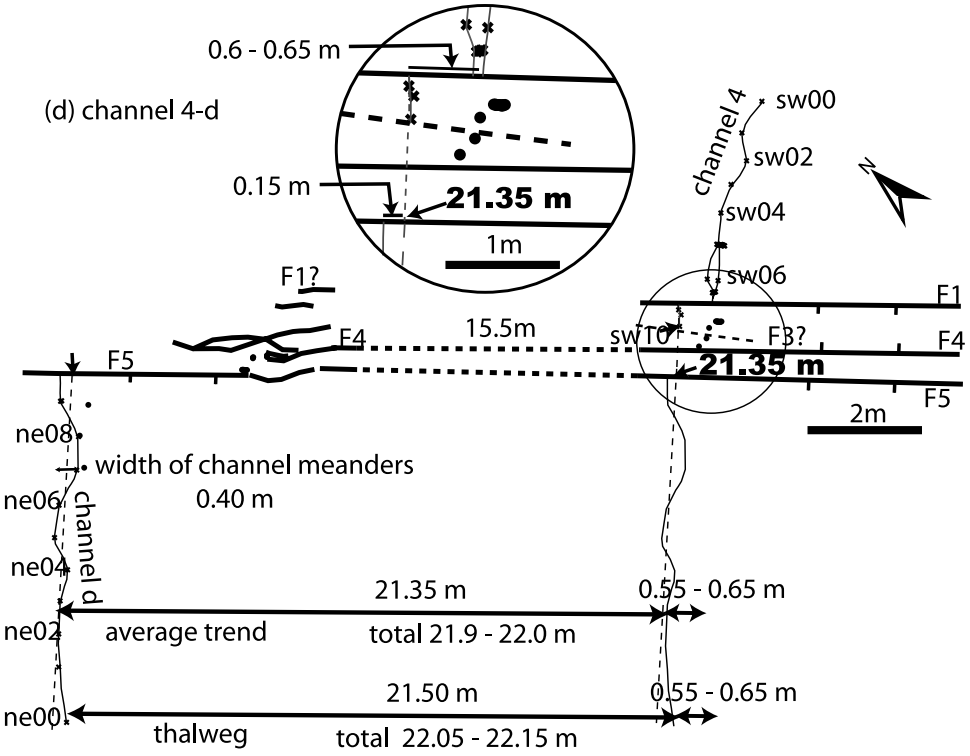


Figure 17. (continued)

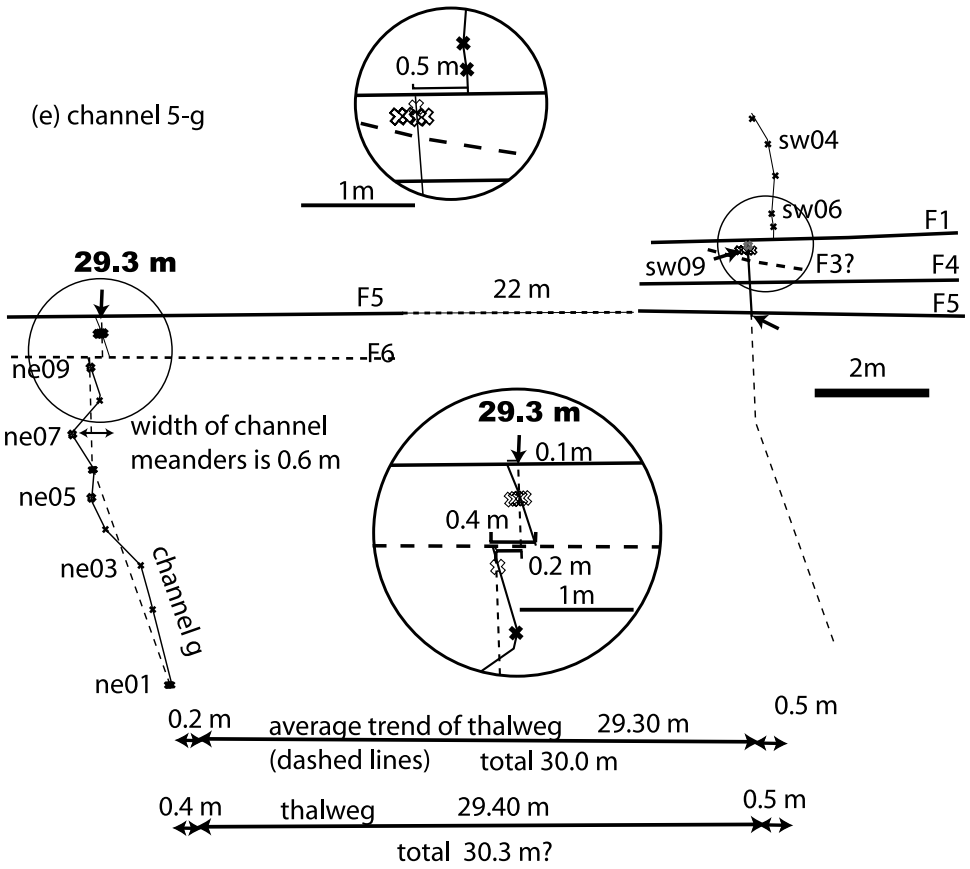


Figure 17. (continued)

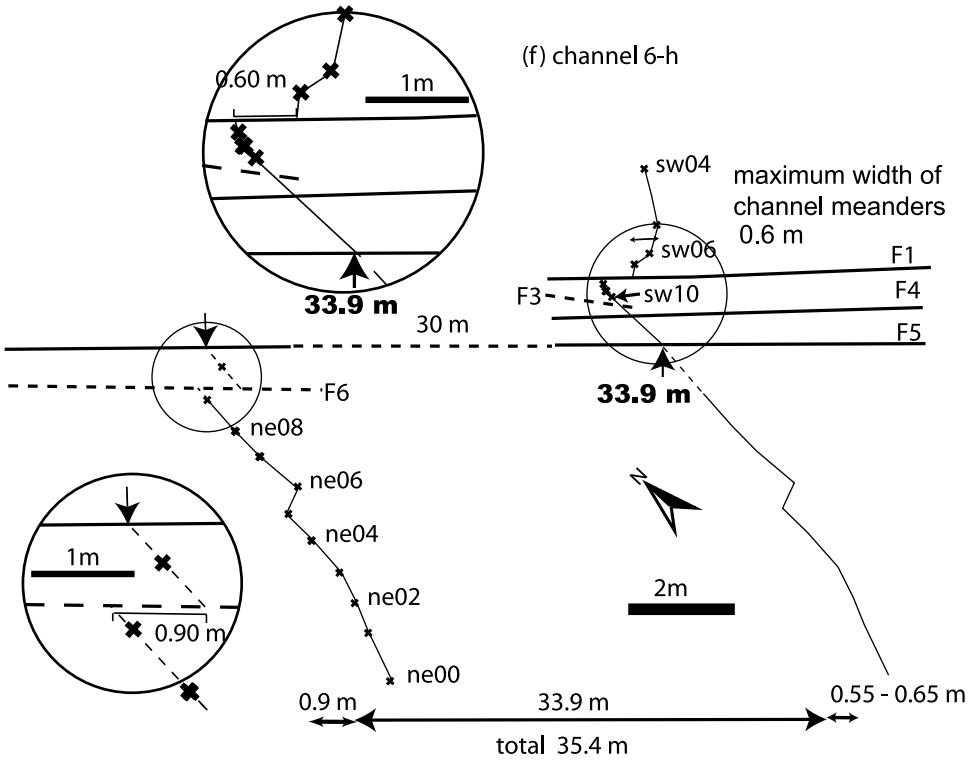


Figure 17. (continued)

surface [*Liu*, 2003, Figure 3.2]. We first discuss the offsets of channels on secondary faults F1 and F2, because these secondary faults appeared to offset channels 1 though 6 a nearly identical amount, about 60 cm (Figure 4g). The slight difference in offset measurable in Figure 4 is likely to reflect uncertainties in measurements, rather than to indicate multiple offset events. Thus F1 and F2 appeared to have slipped only once after the down-cutting of channel 6, probably during the rupture that postdated formation of channel 1. The offset of channel 2 can be ambiguous. Channel 2 was broad and had relatively ill-defined thalweg near F1. Because of this ambiguity, the dextral offset of channel 2 across F1 has a relatively large range of 20–80 cm. However, if channels both older and younger than channel 2 are offset about 60 cm, then channel 2 must also be offset this amount. The abnormal meander of channel 2 immediately downstream from fault 1 could indicate a preexisting fault scarp near fault 1.

6.2. Channel 1-a, 8-m Offset

[63] Two piercing lines constrain the offset of channel 1-a: the deepest thalweg and the basal contact of unit 30 (Figure 17a). The deepest thalweg is offset by F1 and F4 a total of 7.85 m. Our measurements of offset across all three strands have little uncertainty, since our mapping constrains the piercing lines within a couple of ten centimeters to the faults. Hence the extrapolation of piercing lines to the fault yields a trivial uncertainty of only a few cm, at most. The offset of the thalweg of unit 30 is about 8.0 m. Perhaps it is less precise because the location of unit 30 is not clear within 1m of the fault, which implies a greater extrapolation to the principal fault from the downstream segment.

6.3. Channel 2-b, 15.5-m Offset

[64] The deepest thalweg of channel 2-b, very well defined in all trench cuts, provides a superb piercing line delimiting the offset of the channel. This piercing line yields horizontal offsets of 15.30–15.80 m across three strands (Figure 17b). Two other piercing lines yield marginally different ranges of 15.10–15.75 m and 15.20–15.72 m [*Liu*, 2003]. The uncertainty is largely due to about 0.4 m of suspected near-fault warping across F5. Figure 17b shows two interpretations of the offset. If we extrapolate using the trends of the nearest data points, the total offset is at least 15.30 m. However, in the close vicinity of F5, the downstream segment of channel 2-b seemed to arch in a manner suggestive of warping. If the bending is due to warping instead of river meandering, we would have to add about 0.4 m to the offset of simple juxtaposition. Thus the total offset would be about 15.8 m.

6.4. Channel 3-c, 20.7-m Offset

[65] Interpretation of the horizontal offset of channel 3-c involves the restoration of three channel segments along F5 and F4 (Figure 17c). Measurement of offset across F4 produces most of the uncertainty for this channel, because channel c2 trends nearly parallel to the fault zone. If channel c2 turns abruptly into F4 at its southeasternmost exposure (exposure dn4-se06 in Figure 17c blowup), then it is offset 17.65 m from channel 3. If however, the channel c2 thalweg continued toward the southeast before intersecting F4, the offset would be less. A cut 25 cm southeast of exposure se06 of channel c2 constrains the southeasternmost possible extent of the channel. Thus the minimum offset of channels c2 and 3 across F4 is 17.35 m. The offset across F5 is 2.6 ± 0.1 m. To derive the total offset across the fault zone

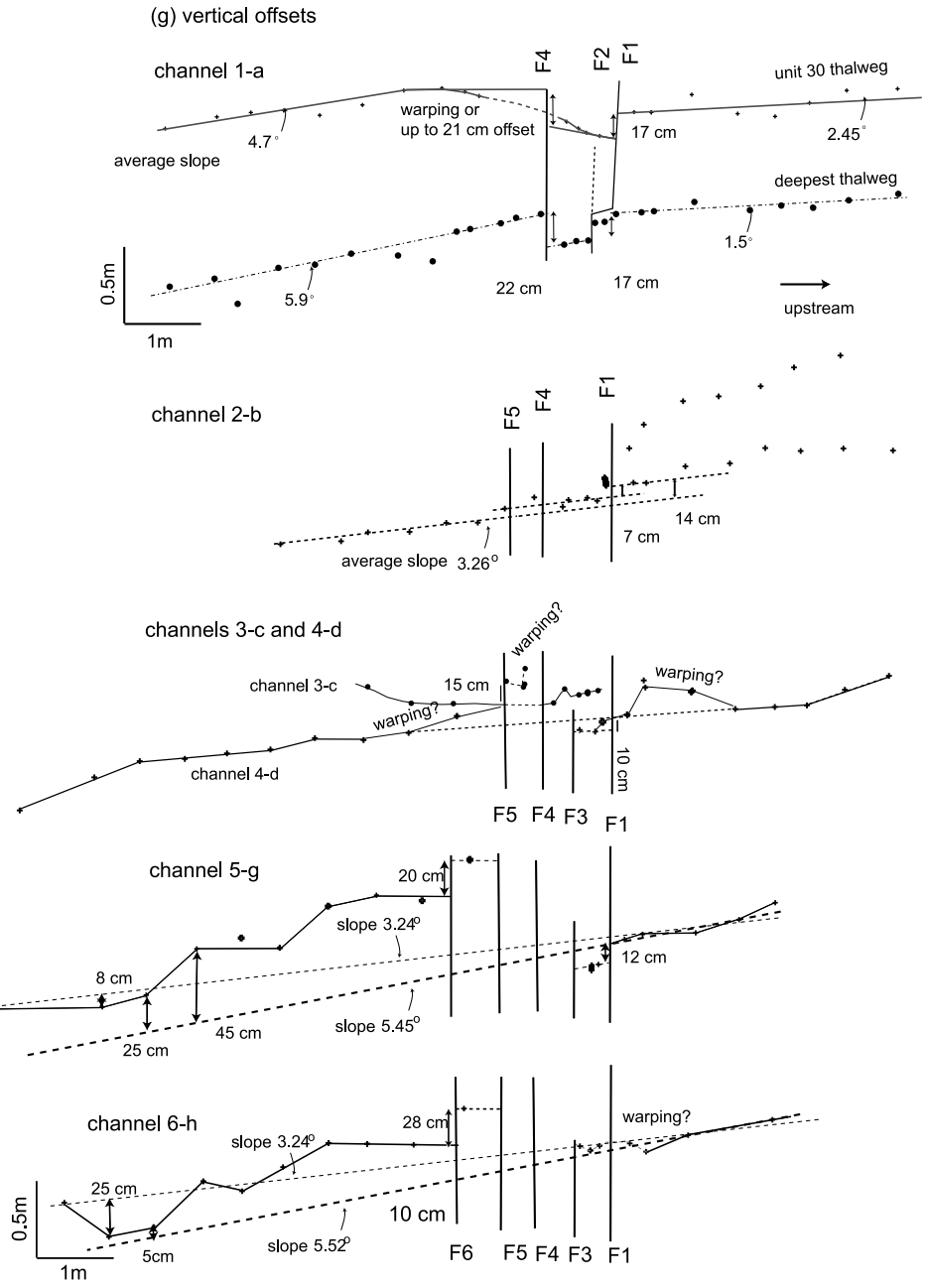


Figure 17. (continued)

since creation of channel 3-c, one must include also the 0.6-m offset of younger channels across F1. The sum of these measurements is 20.7 ± 0.3 m.

6.5. Channel 4-d, 22-m Offset

[66] The best estimation of the lateral offset of the channel 4-d pair is 22.05 ± 0.2 m. This is the combination of measurements using two piercing lines: the thalweg and the average trend. The thalweg suggests a total offset of about 22.1 m, if we use extrapolation between closest exposures of this channel pair (Figure 17d). If instead, we were to use the overall trend of the upstream and the downstream channel segments to extrapolate to the fault zone, the total offset would be slightly smaller, 22.0 m. The 0.2-m uncertainty that we assign to the total offset is half the amplitude of the largest channel meanders exposed in the trenches.

6.6. Channel 5-g, 30-m Offset

[67] Channel 5-g has accumulated about 30.0 ± 0.3 m of right-lateral offset since its creation (Figure 17e). We estimate the error of this measurement to be 0.3 m, half the largest amplitude of channel meanders observed in the excavations of channel g. A slightly larger total offset, 30.3m, is estimated if we extrapolate the thalweg between F5 and F6 using data points closest to the faults. However, this is still within the uncertainty of the previous measurement. We favor the 30.0 ± 0.3 m measurement, because

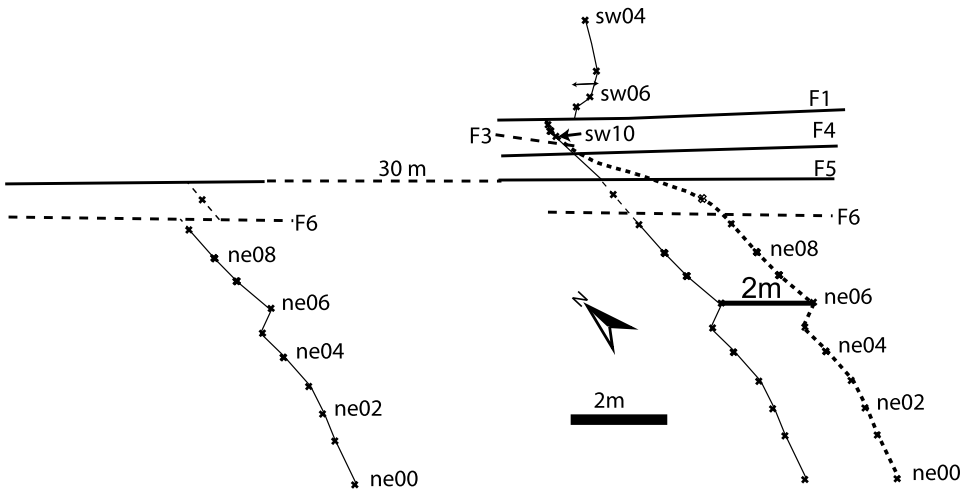


Figure 18. Uncertainty in the offset of channel 6-h. It is ambiguous because this channel intersects the fault zone at an accurate angle, compound by the lack of channel exposure in the fault zone. The solid line indicates the position of downstream channel segment after 35.4 m offset reconstruction. A more accurate intersection of channel with the fault implies larger offset. The dashed line indicates the hypothetical position of downstream segment with an additional 2-m offset.

the general trend of the thalweg provides a longer reference line, and thus a more robust estimation of the offset.

6.7. Channel 6-h, 35.5-m Offset

[68] Channel 6-h appears to record a cumulative right-lateral offset of about 35.4 ± 0.3 m (Figure 17f). However, the maximum plausible offset of this channel is subject to greater ambiguity than that of other pairs, because channel 6 had fault-subparallel deflection in the reach where the channel stratigraphy is missing and the measurement of offset is unusually sensitive to the assumption of initial channel configuration. The 35.4 ± 0.3 m offset, estimated using a straight line extrapolation, should be considered a minimum. A larger deflection of the channel through the fault zone would yield a larger offset value. Shown in Figure 18 as an example, it is not impossible to hide an additional 2m offset. This would yield an offset of 37.4 m. Thus, because of the acute intersection angle of channel 6-h with the fault, the offset is most likely to be substantially more than 35.4 m.

[69] Another source of ambiguity is the offset of channel 6 across F1. Channel 6 curved in the reach immediately upstream from F1. If the curvature were due to channel meandering, the offset across F1 would be 0.6 m. However, if the curvature indicates tectonic warping of a straight channel, then the offset across F1 could be as large as 1.5 m. In favor of the meandering hypothesis, the next older channel 7 ran straight into F1 and displayed no deflection. Furthermore, the strong asymmetry in the shape of channel 6, the southern wall being steeper than the northern wall (Figure 16), is consistent with a channel meander. On the other hand, the curvature of both channels 8 and 9 upstream from F1 suggests strongly tectonic deflection, though it is uncertain whether the event responsible for their deflection is the same as that for channel 6.

6.8. Vertical Offsets

[70] Vertical offsets for individual offsets are always less than 50 cm, but range from northeast-side-up to southwest-side-up (Figure 17g). Cumulative vertical offset is nil. This suggests that geomorphic scarp at the site might be due to juxtaposition of surfaces of different elevations [*Arrowsmith et al.*, 1998] or that earthquakes older than those in this sequence had larger vertical offset. Individual channel long profiles show also the fine structure of the fault zone. For example, channel 1-a suggests the fault zone between F4 and F1 is a graben. Channels 3-c and 4-d indicate that the narrow block between F4 and F5 is a horst. Furthermore, channel profiles are commonly irregular in the vicinity of

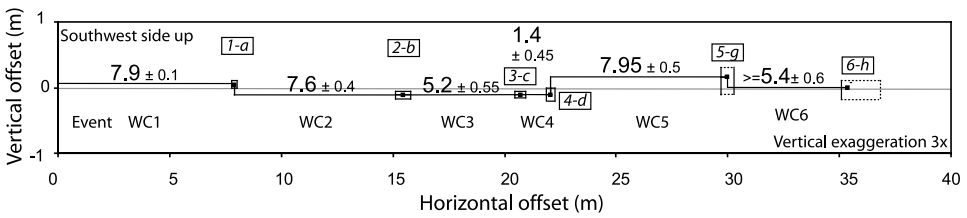


Figure 19. Plot of the offset sequence, using the six channel pairs. The horizontal and vertical offset of each pair appears as a small black rectangle, the size of which indicates the error associated with each measurement. The dextral offsets for the six discrete ruptures are shown by the numbers. The vertical component of slip is in all cases a small fraction of the dextral offset.

the fault zone, an indication of warping, or the presence of pressure ridges associated with brittle faulting.

6.9. Nonbrittle Warping

[71] Warping is prominent in a vertical plane. It is commonly indicated by the anomalous gradient in long profiles of the channels, particularly channels 3, 4, 5 and 6, within or in the vicinity of the fault zone (Figure 17g). This is consistent with the appearance of a large mole track, i.e., welts, mounds and troughs along the surface rupture of an earthquake. However, we found no significant warping in horizontal offsets within the aperture of our excavations, except a possible 0.4 m warp in channel 2-b (Figure 17b). In all other channels, there were not noticeable systematic deviations in plan view of the alignments of channel thalwegs that we can attribute to nonbrittle warping. We suspect that the warping component is probably less than half the amplitude of channel meanders within our excavation aperture. However, if warping is widely distributed away from the main fault zone [e.g., *Rockwell et al.*, 2002], then we would have underestimated the total warping. Thus, from a conservative point of view, the offset amounts we deduce from our excavation should be considered minima.

7. Derivation of a Rupture Sequence

[72] The total dextral offset of $\geq$35.4 m accumulated in six increments. They are 7.9 ± 0.1, 15.5 ± 0.3, 20.7 ± 0.2, 22.05 ± 0.2, 30 ± 0.3 and $\geq$(35.4 ± 0.3). The differences between these values yield the magnitude of the six incremental offsets. From youngest to oldest these are 7.9 ± 0.1, 7.6 ± 0.4, 5.2 ± 0.6, 1.4 ± 0.5, 8.0 ± 0.5 m and $\geq$(5.4 ± 0.6) (Figure 19). For ease of reference, the increments of offset are named WC1 (the youngest) to WC6 (the oldest). Note that at least three of the six increments are within 7.5–8 m, but two consecutive offsets, WC3 and WC4, are about 5.2 and 1.4 m.

7.1. Is Each Offset a Single Rupture Event?

[73] To determine a rupture history for this site along the San Andreas fault, we must consider how many rupture events this sequence of incremental offsets represents. Although a one-for-one correlation may exist, it must be supported by the details of the stratigraphy and geomorphology. Could it be that two separate ruptures occurred within a period during which no new channels were incised? Is it possible that one of the offsets represent two ruptures, one of which was only a few centimeters or a few tens of centimeters?

[74] The completeness of the Wallace Creek paleoseismic record is a function of the number and duration of hiatuses in the record of alluviation and channelization. Hiatuses in either deposition or erosion that occur between rupture events would result in the events not being recorded in the excavated volume. If seismic ruptures have occurred more frequently than alluviation or erosion, then some of the ruptures would not be differentiable in the geologic record. For example, between 35 and 50 m northwest of the upstream channels there are no downstream correlatives to the upstream channels. It is reasonable to propose that a hiatus in deposition and erosion occurred at the site when that 15-m section was in front of the channel. The completeness of the record is also a function of the size of ruptures relative to the size of the depositional and erosional features in the excavated volume and the spacing of our serial excavations. The width of a channel may set the limit of the offset that can be detected at the site. For example, we probably would not recognize a 10-cm offset event, if the channel is 1 m wide. However, if the offset is more than half the width of channel, and if alluviation is frequent enough, the offset event should be recognizable. We turn now to specific discussions of each of the offset channel pairs.

7.2. Offset WC1 and the 1857 Earthquake

[75] The 1857 earthquake is known to have involved rupture of this portion of the San Andreas fault [*Wood*, 1955; *Agnew and Sieh*, 1978], with 8 to 10 m offsets [*Wallace*, 1968; *Sieh*, 1978]. Three-dimensional excavations a few kilometers to the southeast of our site yielded a sharp offset of about 7 m, which has also been ascribed to the 1857 rupture [*Grant and Sieh*, 1993]. None of these geomorphic or stratigraphic offsets can include more than a few centimeters of creep in the past century, since fences constructed in 1908 a few kilometers to the northwest show no misalignments [*Brown and Wallace*, 1968]. Thus it appears that all or at least most of offset WC1 is attributable to slip in 1857.

[76] The geometry and stratigraphy of channel 1-a indicate that all but a few tens of centimeters of the 7.9-m offset must be associated with the 1857 event. Channel 1-a is offset very abruptly across the fault zone. On both sides, we have traced the channel to within 20 cm of the main fault strands. The width of channel 1, which is about 50 cm wide near the fault, also argues that events of more than 50 cm offset could not have occurred during the initial stage of the down-cutting of channel 1.

7.3. Offset WC2 and the Penultimate Rupture

[77] Several observations suggest all or nearly all of the 7.5-m offset WC2 accrued in one event. First, similar to channel 1-a, channel 2-b is offset sharply across the fault. We have traced the channel to within a couple of ten centimeters of the main fault strand. If there had been an offset of the channel greater than a 20 cm or so after initial incision and before filling of the narrow lower portion, the stratigraphy in channel 2-b would not have been continuous up to and across the fault zone. Near the fault zone, we would have expected to see collapse debris from the scarp within the sequence. Furthermore, an event in the early stages of channel filling would have led to development of a channel meander at the fault. Such a meander would be apparent in the map of the channel thalweg and walls. There is also no evidence for a second large event in the shape of the upper units of the channel fill.

7.4. Offsets WC3 and WC4

[78] The channels that define offsets WC3 and WC4 provide a good example of how multiple offsets of a channel can be discriminated if the stratigraphic and geomorphic record is adequate. The upstream channels (3 and 4) sat adjacent to each other and the downstream channels (c and d) occupied the same channel, except near the fault (Figures 4c and 4g). Whereas the older channel (d) flowed straight across the fault in a deep channel, the upper channel (c) left the fault at an angle, and merged

with the straight channel 1 m or so downstream. Channel 4-d had been offset 1–2 m when channel 3-c was incised. This small offset, WC4, is indicated by the difference in the offsets of channel 4-d and channel 3-c. The fact that channel c cut across the upper right of channel d and caused the asymmetrical cross section of d is additional evidence for a corner-cutting deflection after channel 4-d was offset a meter or two.

[79] We do not see any evidence suggesting that the 1- to 2-m offset of 4-d accumulated through multiple events. There is no asymmetric widening of the channel wall of 4-d that we can attribute to faulting, except as it relates to channel c. The double thalwegs of channel 4 and channel d appear to indicate an asymmetric widening. However, since that they are in the same direction on both sides of the fault, the widening is clearly not a response to offset. One would expect that after an offset, the upstream channel would widen in a direction opposite to that of the downstream segment.

[80] It is possible, but there is no evidence, that the 5- to 6-m offset of WC3 represents multiple events. There is only one cut-and-fill sequence within channel 3-c, so evidence of multiple offsets could be hidden in the colluvium that overlies the channel.

7.5. Offsets WC5 and WC6

[81] There is more uncertainty whether the offset WC5 represents a single event. The shallow depth and simple cut-and-fill sequence of channel 5-g may indicate that channel 5-g was incised during a period with less frequent storms. If it is the case, then the possibility of a hiatus in alluviation (and a missing rupture event) is greater for channel 5-g than other channels. Nonetheless, WC5 appears to be due to a single event. Channel 5-g ran into the fault zone at a high angle. The next younger channel, channel 4-d also crossed the fault zone at nearly a right angle. Both upstream and downstream segments were less than 1m wide near the fault.

[82] WC6 is perhaps the most uncertain case, because of the poor stratigraphy and asymmetric shape of channel 6-h. The downstream channel h was about 1m wide in the immediate vicinity of the fault zone; the cross section of channel h was asymmetric toward the south (Figure 4d). This geometry would be consistent with widening of a downstream channel after being right-laterally offset. However, poorer preservation of channel stratigraphy in the upstream reach prevents us from a more rigorous assessment of this possibility.

[83] In summary, abrupt terminations of channel walls and channel stratigraphy at the fault strongly suggest that they the channels were offset in sudden events after they had been at least partially filled. The steep channel walls and the lack of corner-cutting deflections in channel stratigraphy also suggest that most, if not all of the six offsets represent single events, rather than the multiple smaller events. Channels were narrow, about 1m or less. This indicates that events with more than 1 m can be discriminated if the stratigraphic and geomorphic record is adequate.

[84] We cannot argue, however, that hiatuses in either deposition or erosion would result in incomplete record. However, the large depth, 0.7 m or more, and multiple sets of cut-and-fill sequences within channels indicate that alluviation is frequent (once every a few tens of years?). At least, the quiescent period between rupturing events are long enough to allow these channels to stabilize. A quantitative assessment of the frequency of significant storms vs. rupture events would certainly help to resolve the issue of completeness of offset record. This depends on the abundance and quality of datable materials.

8. Radiocarbon Constraints

[85] Radiocarbon analyses of samples from the excavations allow us to place some constraints on the dates of the ruptures. Numerous tiny fragments of detrital charcoal were embedded in many strata, particularly in poorly sorted coarse debris or in well-sorted fine-grained suspended load sediments. Charcoal grains were mostly small and flaky in appearance; only a small percentage of the samples were large enough to be dated by accelerator mass spectrometry (AMS). Since few of charcoal grains were large enough to be dated individually, we also extracted and consolidated charcoal fragments from bulk samples of sediment collected from exposures where tiny charcoal grains were apparent to the naked eye. We also found several burn horizons in the excavations. These generally consisted of a concentration of tiny charcoal fragments in sediment displayed a baked, reddish color. Dates from samples from a burn horizon are generally considered to be a better approximation of the age of a stratum than detrital charcoal, because they are more likely to have burned in situ, rather than been transported to the site from a burn elsewhere.

[86] We selected 27 carbon samples from a collection of over 70 for radiogenic ^{14}C analysis. The results of dated samples are summarized in Figures 20 and S9. Only six samples were from the downstream side, including two embedded in the underlying bedrock of late Pleistocene alluvium; the majority of samples were from the upstream trench.

[87] Inheritance is a common problem in analyses of detrital charcoal. Charcoal may be transported and incorporated into a stratum long after death of the plant. The result is an age that is older than the stratum from which it comes. Inheritance is clearly demonstrated in several cases at the site. For example, U7-20(1) and U7-20(2), which are in the same suspended load layer in channel 8 and only 85 cm apart in the same trench exposure, yielded ages 500–600 years apart (calibrated ages of 2550 ± 190, 2σ range, years B.P. and 3195 ± 165 years B.P., respectively) (Figures 20 and S10). Disconcordant ages within individual strata and stratigraphic inversion of ages are common [e.g., *Rockwell et al.*, 2000; *Vaughan et al.*, 1999; *Rubin and Sieh*, 1997; *Grant and Sieh*, 1993, 1994; *Nelson*, 1992; *Blong and Gillespie*, 1978]. At the Phelan fan site, 5–6 km southeast of the Wallace Creek site, *Grant and Sieh* [1993] reported radiocarbon dates on samples from the same stratum that differed by more than 500 years. At the Bidart fan site, a 2-m-thick section that was probably deposited in 2–3 centuries, contain charcoal samples with similar or stratigraphically inverted ages [*Grant and Sieh*, 1994].

[88] Despite the clear discrepancies, our radiocarbon ages provide some constraint on the dates of the rupture events. The stratigraphic locations of each of the six rupture events appear as thick horizontal lines in Figure 20. The horizontal positioning and length of the line indicates the age range of the event. A quick glance at the relationship of the event

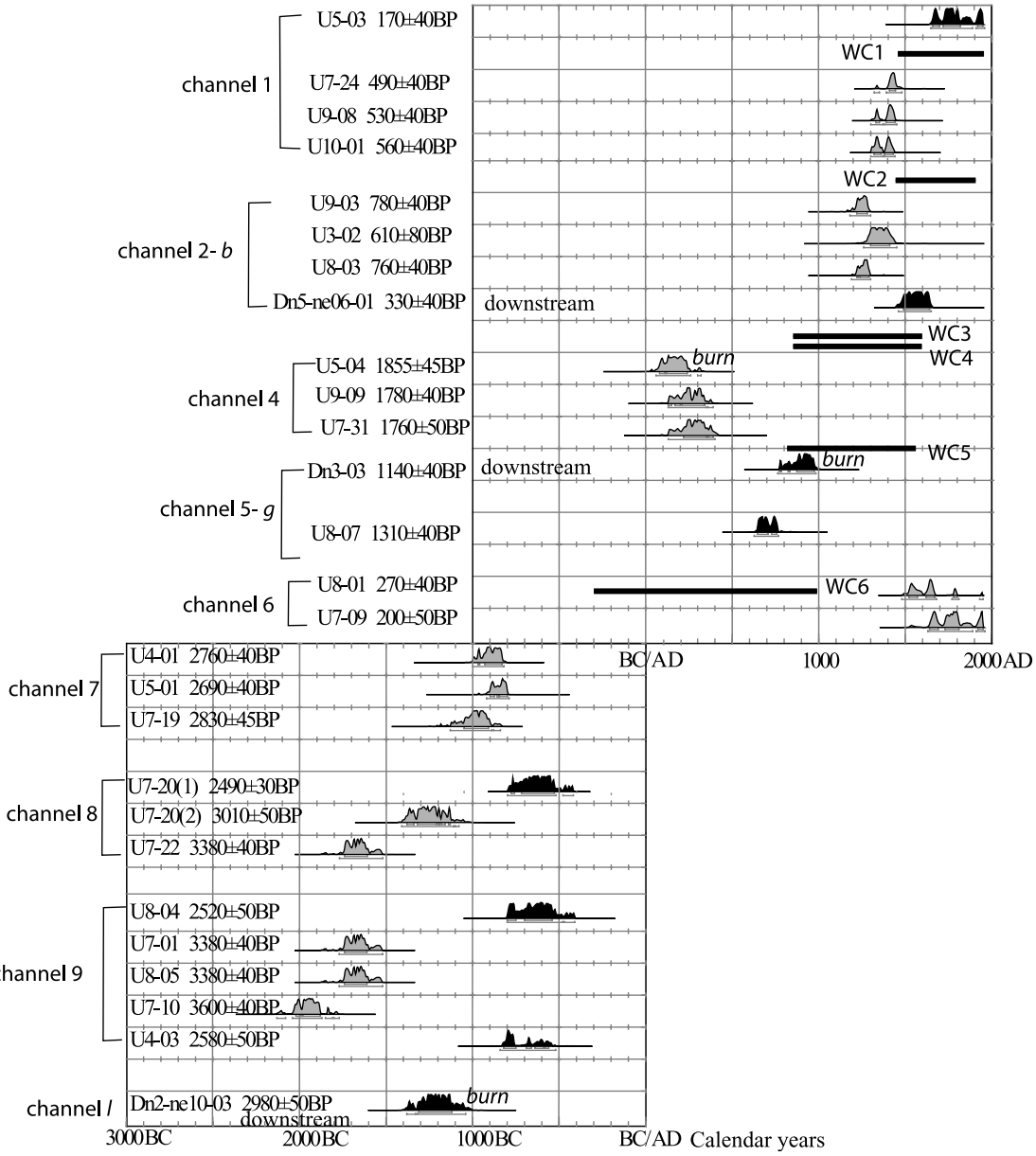


Figure 20. Radiocarbon date ranges of samples from the Wallace Creek site plotted as a function of age and stratigraphic order. The age ranges that we judge to be the most reliable and used to constrain event dates are black, whereas other ages are gray. Justification of the selection of the reliable dates and rejection of the others is given in detail by *Liu* [2003, chapter 3, section 3.6.2]. In general, one can see that the dates we consider to be reliable are the youngest ones. Bars under the age ranges are 1σ and 2σ ranges. OxCal program version 3.5 [*Ramsey*, 1995, 2000] uses atmospheric data from *Stuiver et al.* [1998]. Also shown are the stratigraphic positions of rupture events WC1 through WC6. The horizontal bars indicate their date ranges.

horizons and the black constraining date ranges shows that the ages of the events are poorly constrained. Our highly channelized and bioturbated stratigraphy provides little opportunity to refine the event dates by stratigraphic means [e.g., *Biasi et al.*, 2002] much beyond an averaging of the upper and lower bounding dates.

9. A History of the Latest Six Ruptures

[89] An offset history using dates and offset measurements at the Wallace Creek site is shown in Figure 21. The magnitude of the offsets in this history is more tightly constrained than their dates of occurrence. Constraints on the dates of the events are too poor to allow us to answer any of the important questions about recurrent behavior. Millennially averaged slip rates derived from the data range between 20 and 55 mm/yr, and we have no basis for discussing variability of recurrence within the past two millennia.

[90] Fortunately, previous paleoseismic investigations at the Phelan Creeks and Bidart fan sites, just a few kilometers to the southeast offer an opportunity to narrow the uncertainties.

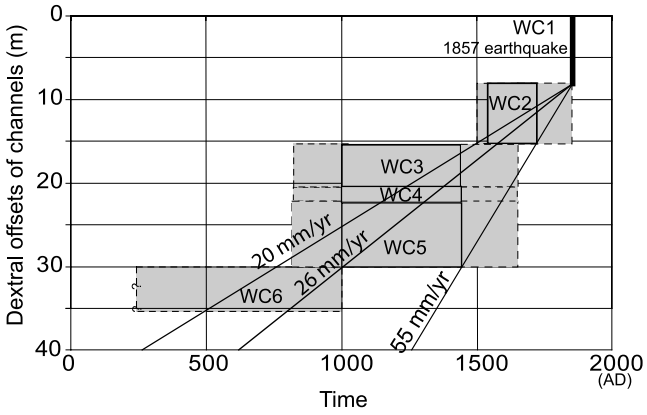


Figure 21. Tentative slip history of the Wallace Creek paleoseismic site for the last 1500 years, based solely on data from the site. The vertical dimensions of the boxes indicate the magnitude of slip in each event. Errors in slip magnitude are too small to show clearly at this scale. The horizontal dimensions of the gray boxes represent the age constraints of the events, solid lines denoting 1σ uncertainties and dashed lines indicating 2σ uncertainties. An average slip rate of 26 mm/yr is shown only for reference.

9.1. Correlation With the Phelan Creeks Site

[91] The Phelan Creeks paleoseismic site lies just 1.5 km southeast of our site (Figure 1b). It has a series of cuts and fills that may correlate with our channel cuts and fills. If so, we can benefit from the correlations, because the radiocarbon dates from the Phelan Creeks site appear to be less plagued by problems of inheritance (Figure S13; J. D. Sims et al., unpublished manuscript, 1994). The Phelan Creeks site was excavated in the 1980s [*Sims*, 1994; J. D. Sims et al., unpublished manuscript, 1994], although its sequence of offsets was first described by *Wallace* [1968]. The site encompasses two active channels, Little Phelan Creek and Large Phelan Creek. The morphology of the channels, aided by a few excavations, revealed that the Little and Large Phelan Creeks are offset 15.8 ± 0.6 m and 17.4 ± 1.6 m, respectively.

[92] A beheaded channel lies about 110 m to the northwest of Little Phelan Creek (channel HC of J. D. Sims et al. (unpublished manuscript, 1994)) [*Liu*, 2003]. Within the fault-parallel segment of the abandoned paleochannel, trenches revealed five distinct cut-and-fill episodes that occurred immediately prior to abandonment of the channel (J. D. Sims et al., unpublished manuscript, 1994). These units occurred on both sides of the fault zone. The ages of these units were comparatively well dated, but the amount of offset of each of these cuts and fills was not documented.

[93] We are intrigued by the fact that the alluvial history of the past 3000 years at Phelan Creeks is remarkably similar to the channel history at the Wallace Creek site (Figure 22). The resemblance is manifest in several aspects. First, both the timing and amount of offset of the modern Phelan Creeks are consistent with those of channel 2-b at the Wallace Creek site. Channel 2-b was incised shortly before a date within the range A.D. 1460–1600 and is offset 15.4 m. The beheaded channel at the Phelan Creeks site was abandoned at the time of incision of the Little and Large Phelan Creeks, which subsequently have been offset about 16 m, respectively. The time of the abandonment was shortly after a date within the range A.D. 1300–1440. Thus the maximum bound on the age of the 16-m offset is constrained by these youngest dates in unit HC-4 within the abandoned channel. Second, both the Phelan Creeks and at Wallace Creek sites exhibited four cuts and fills between about A.D. 500 and 1450. At Phelan Creeks, these were the 4 unconformity-bounded sedimentary units in paleochannel HC. At Wallace Creek, these were channels 3 through channel 6.

[94] A third similarity between the Phelan Creeks and Wallace Creek records is the existence of a long hiatus in erosion and deposition in the centuries before and after A.D.

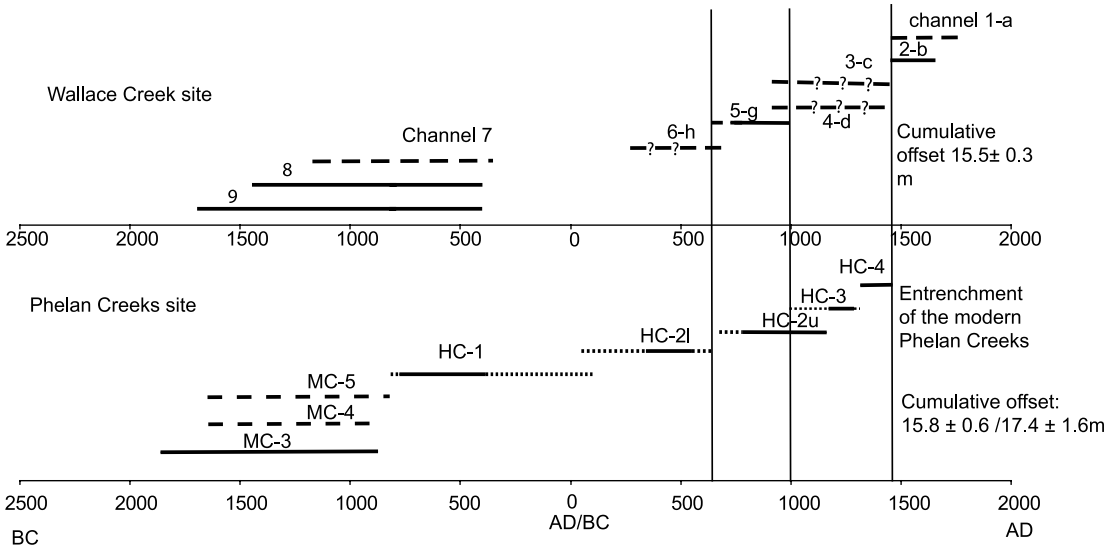


Figure 22. A proposed correlation of the alluvial history at the Wallace Creek site with that at the Phelan Creeks. Horizontal lines represent the age ranges of alluvial events, which are less certain where dashed. The six cut-and-fill events of the past 1500 years at both sites could well be correlative, as could the long hiatus in alluviation and incision centered on A.D. zero.

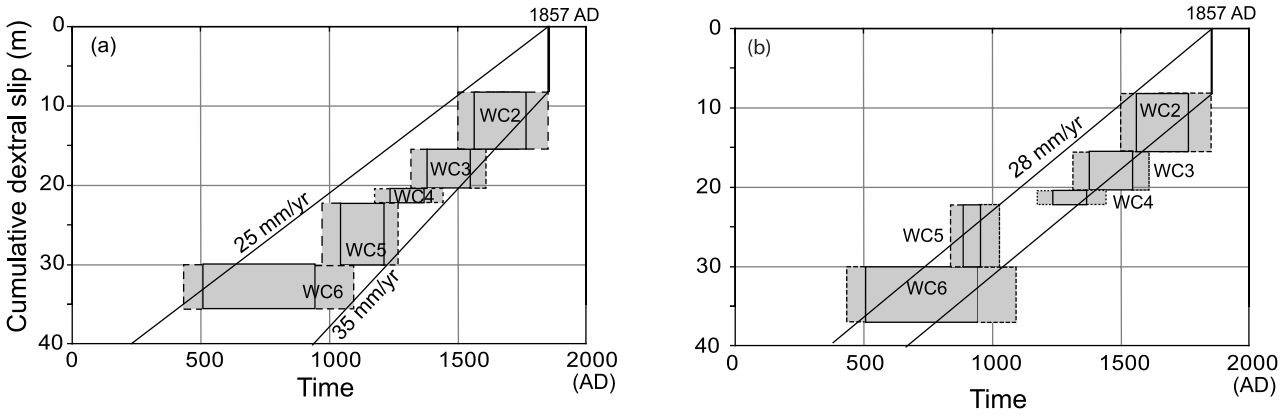


Figure 23. (a) and (b) Different scenarios of a revised slip history for the Wallace Creek site, incorporating age constraints from the nearby Phelan Creeks site. Substitution of age constraints on alluvial events at the Phelan Creeks yields tighter constraints on the dates of paleoseismic events than those derived solely from the Wallace Creek dates (Figure 21). The horizontal dimensions of the gray boxes represent the age constraints of the events; solid lines denoting 1σ uncertainties and dashed lines indicating 2σ uncertainties. Two diagonal lines represent the best estimation of average slip rate; the upper one indicates a slip-predictable idealization, and the lower one indicates a time-predictable idealization. Figures 23a and 23b are identical expect for event WC5.

zero. At Phelan Creeks, this was a 500- to 1000-year hiatus prior to HC-2l. At the Wallace Creek site, the hiatus occurred prior to incision of channel 6-h and after cutting and filling of upstream channel 7. This hiatus corresponded to the long downstream stretch that lacked downstream channels between channels h and i (Figure 4f). This hiatus appears to exist at late Holocene sites elsewhere in southern California, as well. For example, excavations across the Garlock fault, southeast of the Carrizo Plain, showed an extremely low sedimentation rate and less frequent flooding events during the same period [*McGill and Rockwell*, 1998]. Also during the same time period, Walker Lake in west Nevada became shallow and probably desiccated [*Benson et al.*, 1991]. We also find that channel incision at the Wallace Creek and Phelan Creeks sites during the last 1500 years mimic remarkably well the highstands of the Mono Lake [*Stine*, 1990] in eastern California [*Liu*, 2003]. This suggests the alluvial histories have been climatically regulated.

9.2. Revised Dates of Wallace Creek Events Using Phelan Creeks Dates

[95] We infer the ages of some channel fills at Wallace Creek to be the same as those of the sedimentary units at Phelan Creeks. Channel 3-c strata at the Wallace Creek site and correlative Phelan Creeks unit HC-4 would have been deposited about A.D. 1300–1440. Channel 4-d and correlative unit HC-3 would have formed about A.D. 1000–1300 (Figure 22).

[96] If these correlations are correct, the uncertainties in the dates of the offset events WC3, WC4 and WC5 can be narrowed by using tighter bounding ages from Phelan Creeks (Figure 23 and Figure S15). The age of the fifth event WC5, however, is still ambiguous. Figure 23a shows the offset-time plot based on surrogate dates strictly from the Phelan Creek site.

[97] In this scenario, WC5 occurred within the 2σ range of A.D. 970–1270. In the second and less favored scenario, we assume that our sample Dn03-03, an in situ burn, postdates the abandonment of channel 5, thus provides an upper bounding date for WC5. WC5 would have occurred within the 2σ range of A.D. 870–1020 (Figures 23b and S15). Although this age range overlaps with the previous estimation of A.D. 970–1270 within the 2σ uncertainty, the second estimation is significantly older than the first, particularly if one considers the corresponding 1σ age range. This ambiguity may have important implication: the second interpretation of age constraints suggests a slip time pattern more irregular than the first; it also implies a lower slip rate.

[98] The correlation in alluvial history at the Wallace Creek and the Phelan Creeks sites also supports our tentative channel match of channel 6-h: channel 6-h could have been incised about A.D. 250–540. The date of subsequent offset event WC6 still is highly uncertain; it probably occurred sometime between the 6th and 10th centuries (Figure 23).

9.3. Further Constraints From the Bidart Fan Record

[99] The Bidart fan paleoseismic site is on an alluvial fan about 5 km southeast of the Wallace Creek site (Figure 1b).

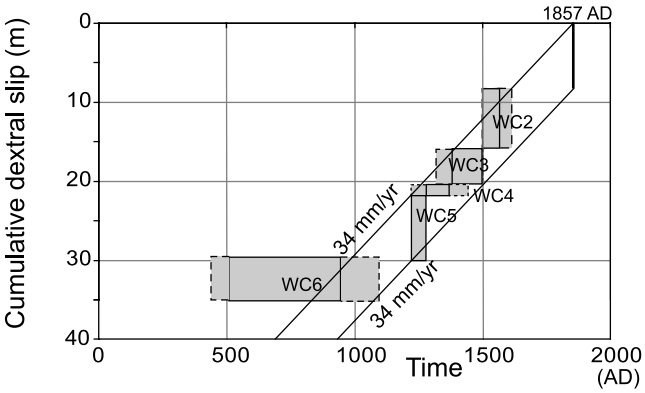


Figure 24. Additional constraints from the Bidart fan site [*Grant and Sieh*, 1994], which further improve the precision of the slip history.

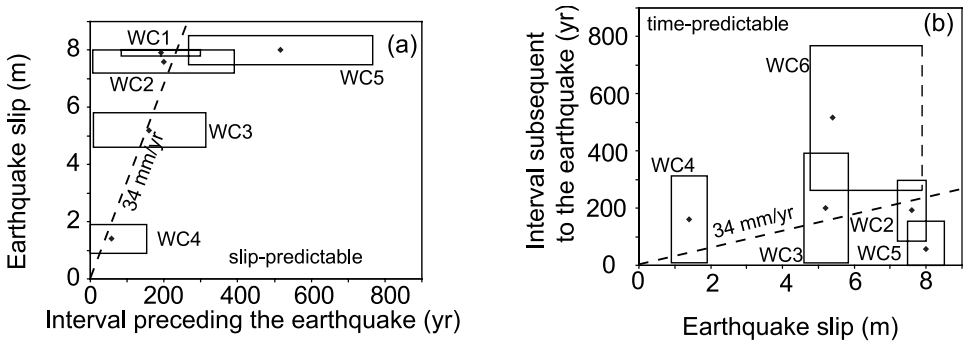


Figure 25. A test of (a) slip-predictable model and (b) time-predictable model, assuming the 4000-year average strain accumulation rate of 34 mm/yr. In Figure 25a, earthquake slip is plotted against the time since the previous earthquake. The slip-predictable model seems to be a good idealization. WC1 through WC4 appear to fall around the dashed line. The poor fit of WC5 could be due to the poorly constrained age of WC6. In Figure 25b, the time interval between two consecutive ruptures is plotted against the slip of the first event. If earthquake occurrence were time-predictable, the points should fall on the dashed line. The time intervals are calculated using 1σ range of events.

Grant and Sieh [1994] documented a sequence of 5 ruptures of the San Andreas fault there, since about A.D. 1200. The latest two events at the Bidart fan (their events A and B) occurred after a date in the range A.D. 1450–1510, and possibly within this range. *Grant and Sieh* [1994] concluded that a gully offset 15 to 18 m at the site represented the cumulative offset of these latest two events, and possibly a third event. The similar magnitude of this offset to the two-event offsets at Wallace Creek and Phelan Creeks suggests that it was the cumulative offset of two events. Radiocarbon dates constrain their other three events (C, D, and E) to have occurred within the period A.D. 1218–1510, with the oldest event (E) being tightly constrained to the period A.D. 1218–1276.

[100] The age constraints from the Bidart site may provide further limits on the date of the five events at Wallace Creek. If the record at the Bidart Fan site is complete for the past five ruptures and if the record at the Wallace Creek site is similarly complete, then their fifth event back (E) would correlate with our event WC5. We would then be able to use the date constraints for event E to bound the date of WC5. Figure 24 shows this modification to the plot of cumulative slip versus time.

10. Discussion and Conclusions

[101] We have recovered from three-dimensional excavations at the Wallace Creek site a well-constrained sequence of the six most recent offsets of the San Andreas fault. Together, they have produced the latest $\geq$35.5 m of dextral offset. We conclude that the dextral slips associated with the latest six events are, from oldest to youngest, $\geq(5.4 \pm 0.6)$, 7.9 ± 0.5, 1.4 ± 0.5, 5.2 ± 0.6, 7.6 ± 0.4 and 7.9 ± 0.1 m.

[102] Although it is possible that smaller events have gone unrecognized in this record, we have found no evidence for them. The resolution of the stratigraphy is such that offsets of 10 cm or so could have gone unrecognized. It is reasonable, yet conservative, to set the lower limit of detection of offsets to be about 0.5 m, about one-third the magnitude of offset WC4. However, the sharp intersections of the gully walls and internal stratigraphy with the fault planes argue against the presence of many of these. Even during long periods of dry conditions, during which gullies would not have been cut, the lack of deflection of the immediately predrought channel rules out the possibility of any of the large offsets being the cumulative result of multiple small-offset events.

[103] Constraints on the timing of the six large events from radiocarbon samples within the excavated volumes are poor. Even so, reasonable correlations with better dated depositional events and hiatuses and ruptures from the nearby Phelan Creeks and Bidart fan sites allow us to construct a useful history of rupture. The average slip rate over the span of the past five events (between A.D. 1210 and 1857) has been 34 mm/yr, a rate indistinguishable from the 3700-year average of 33.9 ± 3 mm/yr [*Sieh and Jahns*, 1984]. It is also similar to geodetically determined strain accumulation rates of 31 to 35 mm/yr over a 175 km aperture spanning the fault [e.g., *Lisowski et al.*, 1991; *Feigl et al.*, 1993].

10.1. Implications for Earthquake Recurrence Models

[104] A remarkable feature in the Wallace Creek offset series is that at least half of the offsets are in the range between 7 and 8 m and that five out of six are greater than 5 m. The asymmetry in the distribution does not prove, but certainly suggests that slips at this location do not result from a uniform random process [*Liu*, 2003]. Furthermore, data at the site do not support a power law frequency-size distribution on a smooth fault as generated by some numerical models [e.g., *Carlson and Langer*, 1989; *Ito and Matsuzaki*, 1990; *Shaw*, 1995; *Cochard and Madariaga*, 1996; *Shaw and Rice*, 2000]. For such models, one would expect that at a given location along the fault, 1- to 2-m offsets would occur far more frequently than 7- to 8-m offsets. To the contrary, our data show that large offsets are far more common than small ones.

[105] Incorporation of the dating constraints from the Phelan Creeks and Bidart fan sites allows us to evaluate the relevance of slip- and time-predictable models [*Shimazaki and Nakata*, 1980]. Assuming a 34 mm/yr strain accumulation rate, a slip-predictable model is an acceptable idealization (Figure 25a). WC5 is the only event that would not fit a slip-predictable model; the time interval preceding WC5 is too long to fit the prediction. However, since the occurrence time of WC6 is ill-con-

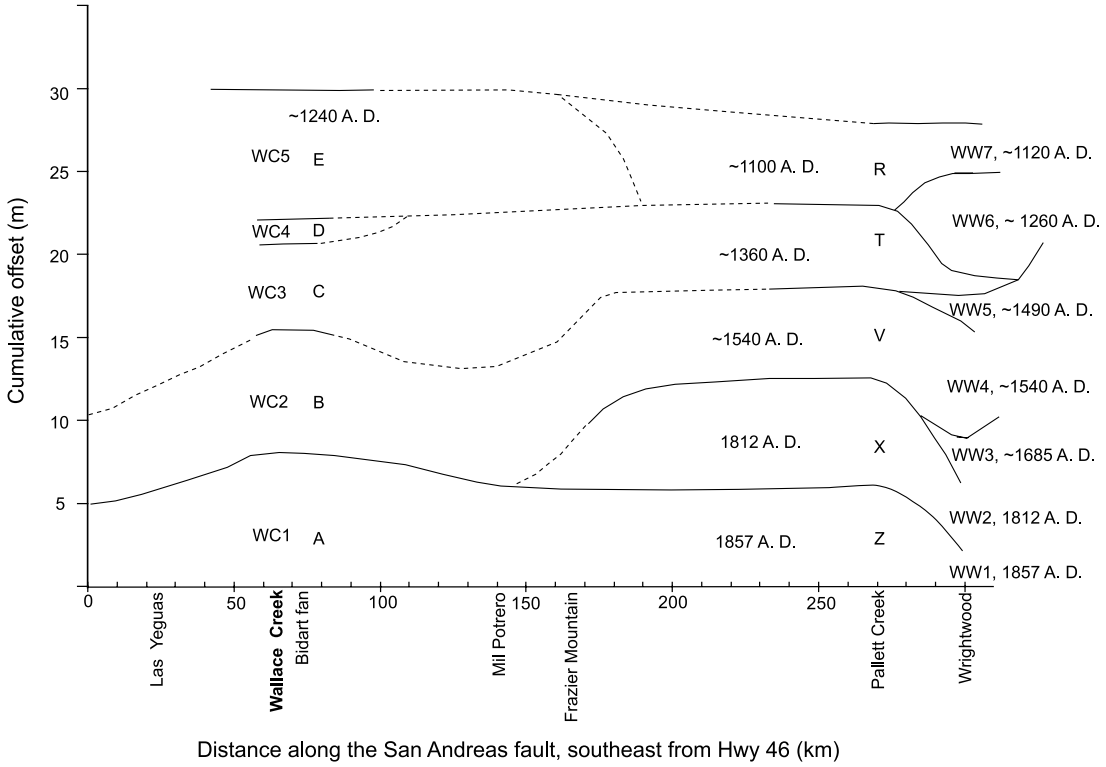


Figure 26. Speculative correlation of earthquake ruptures at the Wallace Creek, the Pallett Creek, and the Wrightwood sites, based on the information of dates of events and slip per events. Data sources for Pallett Creek site are from *Sieh* [1984] and *Salyards et al.* [1992] and for Wrightwood site are from *Weldon et al.* [2004]; slip of the 1857 earthquake is from *Sieh* [1978] and *Lienkaemper and Sturm* [1989].

strained, the time period between WC6 and WC5 could be shorter than the current estimates. A time-predictable model fits the data more poorly than the slip-predictable model (Figure 25b), because of the rapid succession of events WC5, WC4, and WC3. Others have also questioned the applicability of time-predictable models [*Murray and Segall*, 2002; *Weldon et al.*, 2004]. These assessments are important because the time-predictable model is widely used in probabilistic seismic hazard predictions.

[106] Although the dates of the Carrizo Plain events are still too loosely constrained to lend clear support to the slip-predictable model, Figure 25a does show that earthquake slip has a weak but positive correlation with the time interval preceding the earthquake. In particular, large offsets come after long intervals, and small offsets follow short intervals. This contrasts with the interpretation of the Wrightwood paleoseismic site by *Weldon et al.* [2004], 235 km to the southeast on the San Andreas fault. They found a negative correlation between offset magnitude and the period of dormancy prior to a large rupture. The disparity may simply result from different geometric settings of the fault system at the two sites. The Wallace Creek site is located on the central portion of the San Andreas fault, where the fault is geometrically simple. Motion on the San Andreas fault is taken up by a single strand, rather than multiple subparallel strands. Furthermore, 100 km to the north of our site is the Parkfield creeping section of the San Andreas fault, which may serve as a buffer to stop the propagation of ruptures from the north. Thus the Carrizo section of the San Andreas fault may be able to break relatively independently, without influence from the north and from subparallel faults. Near the Wrightwood site, however, the San Andreas fault system is more complex; interference from subparallel faults, such as the San Jacinto fault and Sierra Madre-Cucamonga fault could modulate the earthquake behavior on the San Andreas fault itself [*Palmer et al.*, 1995].

[107] The positive correlation between slip and preparation time at Wallace Creek supports the notion that most accumulated strain is relieved subsequently during large earthquakes. In this sense, the regular occurrence of similar offsets suggests that the concept of the earthquake cycle is most applicable at locations where a fault or fault segment can act independently of other faults [e.g., *Tse and Rice*, 1986; *Ben-Zion*, 1996; *Lapusta et al.*, 2000].

10.2. Correlation of Earthquakes Along the Central San Andreas Fault

[108] Unlike previous correlations along strike, we use both dating constraints on the Wallace Creek site events and the magnitude of slip (Figure 26). We rely principally on data from the Wallace Creek site and the Pallett Creek and Wrightwood sites, because these sites have the longest and best characterized records. One principal constraint on correlations is the number of ruptures that have occurred at the three principal sites since about A.D. 1100. At Wallace Creek, we have documented five events, WC 1 through WC 5. The ages of the events are constrained by history (1857) and by dates of events at the nearby Bidart Fan site. At Pallett Creek, five ruptures have occurred since

about A.D. 1100: events Z, X, V, T, and R. At Wrightwood, six ruptures appear in the record in this same period.

[109] Together, the time and slip constraints from the individual sites suggest that over the past eight centuries, slip has been about uniform along this 220-km reach of the fault (Figure 26). The amount of offset at Pallett Creek may be nearly uniform from event to event, about 6 m each time. Ruptures have been more frequent at Wrightwood, but they have been smaller on average. Furthermore, characteristic earthquakes, with similar rupture extent and slip function, are plausible but not the only form of rupture. Of the most recent five Wallace Creek events, only WC2 may be similar to the 1857 rupture. WC5, though similar in slip to the 1857 event, does not appear to have extended as far south as Pallett Creek.

[110] Some of the correlations suggested in Figure 26 are more speculative than others. For example, we suggest that WC4 propagated into the Wallace Creek site from the northwest and ended a short distance to the southeast. It is also possible that this event actually correlates with event T at Pallett Creek. In that case, it would have extended farther to the south, and later event WC3 would have terminated between Wallace Creek and Pallett Creek. As with every previous correlation chart of paleoseismic events along the San Andreas fault, this one should be viewed as just the latest attempt to make sense of a growing body of paleoseismic information. We hope that more data on both slip timing and magnitude will enable tests of our correlations and eventually lead to a more accurate picture of what has indeed actually occurred.

[111] In conclusion, we have conducted three-dimensional excavations at the Wallace Creek paleoseismic site to reconstruct the slip history at the site. We use stratigraphic evidence for correlating channels across the fault, which is more robust than geomorphologic evidence alone. Closely spaced sequential excavations allow accurate measurements of six pairs of matched channels, with uncertainty on the order of a few tens of centimeters. Evidence suggests strongly that each of the six offset increments represent one rupture event. Thus the right-lateral displacements associated with the last six events are, from youngest to oldest these are 7.9 ± 0.1, 7.6 ± 0.4, 5.2 ± 0.6, 1.4 ± 0.5, 8.0 ± 0.5 m, and $> (5.4 \pm 0.6)$. This offset series does not appear to result from a random process, nor from a simple power law process. Constraints on the timing of these events from radiocarbon samples at our site are poor. However, combination with evidence from the nearby Phelan Creeks and Bidart fan sites, allows construction of a useful rupture chronology. The average slip rate during the last millennial has been 34 mm/yr, a rate indistinguishable from the 3700-year average and geodetic rate. Despite large still uncertainty in age ranges, these events suggest earthquake slip at the site has generally a positive correlation with the time interval preceding the event. Smaller offsets coincide with shorter prior intervals and larger offset with longer prior intervals.

[112] **Acknowledgments.** We thank Brandon Maehr for continuous assistance in hand excavations and surveying and Johna Hurl and Kathy Sharum from the Bakersfield office of the Bureau of Land Management for assisting in getting permission to excavate the site. Most of the excavations were done by hand. Brandon Maehr removed at least half of the excavated 450 m^3 of sediment. Additional field assistance was provided by Jim Nye, Clay Stevens, Chris Madden, and Lingsen Zeng. Clay Stevens and O. C. Canto helped digitize the trench logs. We thank Ramon Arrowsmith and John Sims for sharing an unpublished manuscript that describes the paleoseismic investigation of the Phelan Creeks site and Lisa Grant for discussing ^{14}C dates at the Bidart fan site. Ray Weldon's thorough and critical review helped improve the manuscript. This research was partially supported by U.S. Geological Survey grant 99-HQ-GR-0043 and 01-HQ-GR-0002. The work was also partially supported by the Southern California Earthquake Center (SCEC) and private funds.

References

Agnew, D. C., and K. E. Sieh (1978), A documentary study of the felt effects of the great California earthquake of 1857, *Bull. Seismol. Soc. Am.*, *68*, 1717–1729.

Arrowsmith, R. J., D. D. Pollard, and D. D. Rhodes (1998), Morphological dating of scarps formed by repeated slip events along the San Andreas fault, Carrizo Plain, California, *J. Geophys. Res.*, *103*, 10,141–10,160.

Bak, P., and C. Tang (1989), Earthquakes as a self-organized critical phenomenon, *J. Geophys. Res.*, *94*, 15,635–15,637.

Ben-Zion, Y. (1996), Stress, slip, and earthquakes in models of complex single-fault systems incorporating brittle and creep deformations, *J. Geophys. Res.*, *101*, 5677–5706.

Benson, L. V., P. A. Meyers, and R. J. Spencer (1991), Change in the size of Walker Lake during the past 5000 years, *Palaeogeogr. Palaeoclimatol. Palaeoecol.*, *81*, 189–214.

Biasi, G. P., R. J. Weldon II, T. E. Fumal, and G. G. Seitz (2002), Paleoseismic event dating and the conditional probability of large earthquakes on the southern San Andreas fault, California, *Bull. Seismol. Soc. Am.*, *92*, 2761–2781.

Blong, R. J., and R. Gillespie (1978), Fluvially trasported charcoal gives erroneous ^{14}C ages for recent deposits, *Nature*, *271*, 739–741.

Brown, R. D., Jr., and R. E. Wallace (1968), Current and historic fault movement along the San Andreas fault between Paicines and Camp Dix, California, in *Proceedings of Conference on Geologic Problems of San Andreas Fault System*, edited by W. R. Dickinson and A. Grantz, *Stanford Univ. Publ. Geol. Sci.*, *11*, 22–41.

Carlson, J. M., and J. S. Langer (1989), Properties of earthquakes generated by fault dynamics, *Phys. Rev. Lett.*, *62*, 2632–2635.

Cochard, A., and R. Madariaga (1996), Complexity of seismicity due to highly rate-dependent friction, *J. Geophys. Res.*, *101*, 25,321–25,336.

Dibblee, T. W. (1973), Regional geologic map of the San Andreas and related faults in Carrizo Plain, Temblor, Caliente, and La Panza ranges and vicinity, California, *U.S. Geol. Surv. Misc. Geol. Invest. Map, I-757*.

Feigl, K. L. A., et al. (1993), Space geodetic measurement of crustal deformation in central and southern California, 1984–1992, *J. Geophys. Res.*, *98*, 21,677–21,712.

Gaudemer, Y., P. Tapponnier, and D. L. Turcotte (1989), River offsets across active strike-slip faults, *Ann. Tectonicae*, *3*, 55–76.

Grant, L. B., and K. Sieh (1993), Stratigraphic evidence for seven meters of dextral slip on the San Andreas fault during the 1857 earthquake in the Carrizo Plain, *Bull. Seismol. Soc. Am.*, *83*, 619–635.

Grant, L. B., and K. Sieh (1994), Paleoseismic evidence of clustered earthquakes on the San Andreas fault in the Carrizo Plain, California, *J. Geophys. Res.*, *99*, 6819–6841.

Huang, J., G. Narkounskaia, and D. L. Turcotte (1992), A cellular-automata, slider-block model for earthquakes. 2. Demonstration of self-organized criticality for a 2-D system, *Geophys. J. Int.*, *111*, 259–269.

Huang, W. (1993), Morphologic patterns of stream channels on the active Yishu fault, southern Shandong Province, eastern China: Implications for repeated great earthquakes in the Holocene, *Tectonophysics*, *219*, 283–304.

Ito, K., and M. Matsuzaki (1990), Earthquakes as self-organized critical phenomena, *J. Geophys. Res.*, *95*, 6853–6860.

Lapusta, N., J. Rice, Y. Ben-Zion, and G. Zheng (2000), Elastodynamic analysis for slow tectonic loading with spontaneous rupture episodes on faults with rate- and state-dependent friction, *J. Geophys. Res.*, *105*, 23,765–23,789.

Lienkaemper, J. J., and T. A. Sturm (1989), Reconstruction of a channel offset in 1857(?) by the San Andreas fault near Cholame, California, *Bull. Seismol. Soc. Am.*, *79*, 901–909.

Lindvall, S. C., T. K. Rockwell, K. W. Hudnut, and S. N. Ward (1989), Slip distribution of prehistorical earthquakes on the Superstition Hills Fault, San Jacinto Fault zone, southern California, based on offset geomorphic features, *Geol. Soc. Am. Abstr. Programs*, *21*, 973–974.

Lisowski, M., J. C. Savage, and W. H. Prescott (1991), The velocity field along the San Andreas fault in central and southern California, *J. Geophys. Res.*, *96*, 8369–8389.

Liu, J. (2003), Part I. Slip behavior of the San Andreas fault through several earthquake cycles. Part II. A structural interpretation of the aftershock "cloud" of the 1992 M_w 7.3 Landers earthquake, Ph.D. thesis, Calif. Inst. of Technol., Pasadena.

Liu, J., Y. Klinger, K. Sieh, and C. Rubin (2004), Six similar sequential ruptures of the San Andreas fault, Carrizo Plain, California, *Geology*, *32*, 649–652, doi:10.1130/G20478.1.

Lyakhovsky, V., Y. Ben-Zion, and A. Agnon (2001), Earthquake cycle, fault zones, and seismicity patterns in a rheologically layered lithosphere, *J. Geophys. Res.*, *106*, 4103–4120.

McCalpin, J. (Ed.) (1996), *Paleoseismology*, 588 pp., Cambridge Univ. Press, New York.

McGill, S., and T. Rockwell (1998), Ages of late Holocene earthquakes on the central Garlock fault near El Paso Peaks, California, *J. Geophys. Res.*, *103*, 7265–7279.

Murray, J., and P. Segall (2002), Testing time-predictable earthquake recurrence by direct measurement of strain accumulation and release, *Nature*, *419*, 287–291.

Nelson, A. R. (1992), Discordant ^{14}C ages from buried tidal-marsh soils in the Cascadian subduction zone, southern Oregon coast, *Quat. Res.*, *38*, 74–90.

Palmer, R., R. Weldon, E. Humphreys, and F. Saucier (1995), Earthquake recurrence on the southern San Andreas modulated by fault-normal stress, *Geophys. Res. Lett.*, *22*, 535–538.

Pantosti, D., R. Collier, G. D'Addezio, E. Masana, and D. Sakellariou (1996), Direct geological evidence for prior earthquakes on the 1981 Corinth fault (central Greece):, *Geophys. Res. Lett.*, *23*, 3795–3798.

Prentice, C. S., and K. Sieh (1989), A paleoseismic site along the Carrizo segment of the San Andreas fault, central California, *Eos Trans. AGU*, *70*, 1349.

Ramsey, C. B. (1995), Radiocarbon calibration and analysis of stratigraphy: The OxCal program, *Radiocarbon*, *37*, 425–430.

Ramsey, C. B. (2000), OxCal Program ver. 3.5, Radiocarbon Accelerator4 Unit, Univ. of Oxford, Oxford, U. K. (Available at http://www.rlaha.ox.ac.uk/O/oxcal.php)

Ran, Y., R. Duan, Q. Deng, D. Jiao, and W. Min (1997), 3-D trench excavation and paleoseismology at Gaowanzi of the Haiyuan fault (in Chinese with English abstract), *Seismol. Geol.*, *19*(2), 97–107.

Reid, H. F. (1910), The mechanics of the earthquakes, in *The California Earthquake of April 18, 1906*, *Carnegie Inst. Washington Publ.*, *87*(2), 192 pp.

Rice, J. R. (1993), Spatio-temporal complexity of slip on a fault, *J. Geophys. Res.*, *98*, 9885–9907.

Rice, J. R., and Y. Ben-Zion (1996), Slip complexity in earthquake fault models, *Proc. Natl. Acad. Sci. U. S. A.*, *93*, 3811–3818.

Rockwell, T. K., S. Lindvall, M. Herzberg, D. Murbach, T. Dawson, and G. Berger (2000), Paleoseismology of the Johnson Valley, Kickapoo, and Homestead Valley faults: Clustering of earthquakes in the eastern California shear zone, *Bull. Seismol. Soc. Am.*, *90*, 1200–1236.

Rockwell, T. K., S. Lindvall, T. E. Dawson, R. M. Langridge, W. Lettis, and Y. Klinger (2002), Lateral offsets on surveyed cultural features resulting from the 1999 Izmit and Duzce earthquakes, Turkey, *Bull. Seismol. Soc. Am.*, *92*, 79–94.

Rubin, C. M., and K. Sieh (1997), Long dormancy, low slip rate, and similar slip-per-event for the Emerson fault, eastern California shear zone, *J. Geophys. Res.*, *102*, 15,319–15,334.

Rundle, J. B. (1988), A physical model for earthquakes: 2. Application to southern California, *J. Geophys. Res.*, *93*, 6255–6274.

Salyards, S. L., K. E. Sieh, and J. L. Kirschvink (1992), Paleomagnetic measurement of nonbrittle coseismic deformation across the San Andreas fault at Pallett Creek, *J. Geophys. Res.*, *97*, 12,457–12,470.

Schumm, S. A., J. F. Dumont, and J. M. Holbrook (2000), *Active Tectonics and Alluvial Rivers*, 276 pp., Cambridge Univ. Press, New York.

Schwartz, D. P., and K. J. Coppersmith (1984), Fault behavior and characteristic earthquakes: Examples from the Wasatch and San Andreas fault zones, *J. Geophys. Res.*, *89*, 5681–5698.

Sharp, R. V., et al. (1982), Surface faulting in the central Imperial Valley, in *The Imperial Valley, California, Earthquake of October 15, 1979*, *U.S. Geol. Surv. Prof. Pap.*, *1254*, 119–143.

Shaw, B. E. (1995), Frictional weakening and slip complexity in earthquake faults, *J. Geophys. Res.*, *100*, 18,239–18,252.

Shaw, B. E., and J. R. Rice (2000), Existence of continuum complexity in the elastodynamics of repeated fault ruptures, *J. Geophys. Res.*, *105*, 23,791–23,810.

Shimazaki, K., and T. Nakata (1980), Time-predictable recurrence model for large earthquakes, *Geophys. Res. Lett.*, *7*, 279–282.

Sieh, K. E. (1978), Slip along the San Andreas fault associated with the great 1857 earthquake, *Bull. Seismol. Soc. Am.*, *68*, 1421–1448.

Sieh, K. E. (1981), A review of geological evidence for recurrence times of large earthquakes, in *Earthquake Prediction: An International Review*, *Maurice Ewing Ser.*, vol. 4, edited by D. W. Simpson and P. G. Richards, pp. 181–207, AGU, Washington, D. C.

Sieh, K. E. (1984), Lateral offsets and revised dates of large prehistoric earthquakes at Pallett Creek, southern California, *J. Geophys. Res.*, *89*, 7641–7670.

Sieh, K. (1986), Slip rate across the San Andreas fault and prehistoric earthquakes at Indio, California, *Eos Trans. AGU*, *67*(44), 1200.

Sieh, K. E. (1996), The repetition of large-earthquake ruptures, *Proc. Natl. Acad. Sci. U.S.A.*, *93*, 3764–3771.

Sieh, K. E., and R. H. Jahns (1984), Holocene activity of the San Andreas fault at Wallace Creek, California, *Geol. Soc. Am. Bull.*, *95*, 883–896.

Sims, J. D. (1994), Stream channel offset and abandonment and a 200-year average recurrence interval of earthquake on the San Andreas fault at Phelan Creeks, Carrizo Plain, California., in *Proceedings of the Workshop on Paleoseismology*, edited by C. S. Prentice, D. P. Schwartz, and R. S. Yeats, *U. S. Geol. Surv. Open File Rep.*, *94-568*, 170–172.

Stine, S. (1990), Late Holocene fluctuations of Mono Lake, eastern California, *Paleogeogr. Paleoclimatol. Paleoecol.*, *78*, 333–381.

Stuart, W. D. (1986), Forecast model for large and great earthquakes in southern California, *J. Geophys. Res.*, *91*, 13,771–13,786.

Stuiver, M., P. J. Reimer, E. Bard, J. W. Beck, G. S. Burr, K. A. Hughen, B. Kromer, G. McCormac, J. van der Plicht, and M. Spurk (1998), INTCAL98 radiocarbon age calibration, 24,000-0 cal BP, *Radiocarbon*, *40*, 1041–1083.

Tse, S. T., and J. R. Rice (1986), Crustal earthquake instability in relation to the depth variation of frictional slip properties, *J. Geophys. Res.*, *91*, 9452–9472.

Vaughan, P. R., K. M. Thorup, and T. K. Rockwell (1999), Paleoseismology of the Elsinore fault at Agua Tibia Mountain, southern California, *Bull. Seismol. Soc. Am.*, *89*, 1447–1457.

Wallace, R. E. (1968), Notes on stream channels offset by the San Andreas fault, in *Proceedings of Conference on Geologic Problems of the San Andreas Fault*, edited by W. R. Dickinson and A. Grantz, *Stanford Univ. Publ. Geol. Sci.*, *11*, 6–21.

Ward, S. N. (1997), Dogtails versus rainbows; synthetic earthquake rupture models as an aid in interpreting geological data, *Bull. Seismol. Soc. Am.*, *87*, 1422–1441.

Ward, S. N., and S. D. B. Goes (1993), How regularly do earthquakes recur? A synthetic seismicity model for the San Andreas fault, *Geophys. Res. Lett.*, *20*, 2131–2134.

Weldon, R. J., T. E. Fumal, T. J. Powers, S. K. Pezzopane, K. M. Scharer, and J. C. Hamilton (2002), Structure and earthquake offsets on the San Andreas fault at the Wrightwood, California, paleoseismic site, *Bull. Seismol. Soc. Am.*, *92*, 2704–2725.

Weldon, R., K. Scharer, T. Fumal, and G. Biasi (2004), Wrightwood and the earthquake cycles: What a long recurrence record tells us about how faults work, *GSA Today*, *14*(9), 4–10.

Wood, H. O. (1955), The 1857 earthquake in California, *Bull. Seismol. Soc. Am.*, *45*, 47–67.

Working Group of California Earthquake Probability (1988), Probabilities of large earthquakes occurring in California along the San Andreas fault, *U.S. Geol. Surv. Open File Rep., 88-398*.

Working Group of California Earthquake Probability (1995), Seismic hazards in southern California: Probable earthquakes, 1994–2024, *Bull. Seismol. Soc. Am.*, *85*, 379–439.

Yeats, R., K. Sieh, and C. Allen (1997), *The Geology of Earthquakes*, 568 pp., Oxford Univ. Press, New York.

Y. Klinger, Laboratoire de Tectonique, Institut de Physique du Globe Paris, 4 place Jussieu, F-75252 Paris cedex 05, France.

J. Liu-Zeng, Institute of Tibetan Plateau Research, Chinese Academy of Sciences, 18 Shuang Qing Road, P.O. Box 2871, Beijing 100085, China. (liu-zeng@itpcas.ac.cn)

C. Rubin, Department of Geological Sciences, Central Washington University, Ellensburg, WA 98926, USA.

G. Seitz, Department of Geological Sciences, San Diego State University, San Diego, CA 92182-1020, USA.

K. Sieh, Division of Geological and Planetary Sciences, California Institute of Technology, Pasadena, CA 91125, USA.